Impaired Annulus Fibrosis Development and Vertebral Fusion Cause Severe Scoliosis in Mice with Deficiency of JNK1 and JNK2

Veronica Ulici[1], Kathryn L Kelley[1], Lara Longobardi[1], Margaret A McNulty[2], Eric W Livingston[3], Ted A Bateman[3], Cheryle A Séguin[4], Craig R Louer[5] and Richard F Loeser[1*]

[1]Division of Rheumatology, Allergy and Immunology and the Thurston Arthritis Research Center, University of North Carolina at Chapel Hill, Chapel Hill, NC, USA; [2]Department of Anatomy & Cell Biology, Indiana University School of Medicine, Indianapolis, IN, USA; [3]Joint Department of Biomedical Engineering, University of North Carolina at Chapel Hill, Chapel Hill, NC, USA; [4]Department of Physiology and Pharmacology, Schulich School of Medicine and Dentistry, Bone and Joint Institute, The University of Western Ontario, London, ON, CAN. [5]Department of Orthopedic Surgery, University of North Carolina at Chapel Hill, Chapel Hill, NC, USA.

Running title: Scoliosis in JNK1/2 dKO mice

Funding: Supported by grant R37 AR049003 from the National Institute of Arthritis, Musculoskeletal and Skin Diseases

*__Correspondence to__: Richard F. Loeser M.D., Thurston Arthritis Research Center, University of North Carolina, 3300 Thurston Building, CB #7280, Chapel Hill, NC 27599-7280. E-mail: richard_loeser@med.unc.edu

Disclosures: None declared.

Abstract

MAP kinases, including JNK, play an important role in the development and function of a large variety of tissues. We analyzed the skeletal phenotype of *JNK1* and *JNK2* double knockout (dKO) mice (*JNK1*$^{fl/fl}$*Col2-Cre*/*JNK2*$^{-/-}$) and control genotypes, including single knockouts, at different embryonic and postnatal stages. The *JNK1/2* dKO mice displayed a severe scoliotic phenotype that began during development and was grossly apparent around weaning age. Alcian blue staining of embryos (E17.5) showed abnormal fusion of the posterior spinal elements. In the adult mice, fusion of vertebral bodies and of spinous and transverse processes was noted by microCT, Alcian blue/Alizarin red stain and histology. The long bones developed normally and histological sections of the growth plate and articular cartilage did not reveal significant abnormalities. Histological sections of the vertebral column at E15.5 and E17.5 revealed an abnormal organization of the annulus fibrosus in the dKOs, with chondrocyte-like cells and fusion of dorsal processes. Spinal sections in 10-week–old dKO mice showed replacement of intervertebral disc structures (annulus fibrosus and nucleus pulposus) by cartilage and bone tissues, with cells staining for markers of hypertrophic chondrocytes including collagen X and Runx2. These findings demonstrate a requirement for both JNK1 and JNK2 in the normal development of the axial skeleton with loss of JNK signaling resulting in abnormal endochondral bone formation and subsequent severe scoliosis.

Introduction

The three major mitogen-activated protein kinase (MAPK) pathways that include extracellular signal-regulated kinase (ERK), p38, and c-Jun NH2-terminal kinase (JNK), play an important role in the normal development and function of a large variety of tissues, including cartilage [1, 2]. The JNK MAPK pathway (also known as the stress-activated protein kinase pathway) is activated by a number of stress stimuli such as oxidative stress, inflammatory cytokines, and mechanical loading [3-7], factors that are known to play an important role in musculoskeletal disorders, including osteoarthritis (OA) and intervertebral disc (IVD) degeneration. Similar to the other MAPK pathways, JNK is activated by a protein kinase cascade in which mitogen-activated protein kinase kinase kinases (MEKKs) phosphorylate and activate mitogen-activated protein kinase kinase (MKK) 4 and MKK7 which in turn phosphorylate and thereby activate one or more of the three members of the JNK protein family: JNK1, 2, and 3 [2]. JNK1 and 2 are expressed in most tissues, whereas JNK3 is restricted to brain, heart, and testis [8, 9].

We initiated a project to analyze the role of JNK in OA pathogenesis using mice with deletion of JNK1, JNK2, and both JNK1 and 2. Because combined germ-line deletion of *JNK1* and *2* is embryonic lethal [8], conditional JNK1/2 double knockout (dKO) mice were generated by crossing *JNK1*$^{fl/fl}$ mice with *JNK2*$^{-/-}$ mice and with mice expressing Cre recombinase under control of the type II collagen promoter (Col2-Cre). However, the dKO mice developed a severe scoliotic phenotype, preventing subsequent studies on OA pathogenesis but prompting an investigation into the role of JNK1 and JNK2 in development of the spine.

A role for JNK in spine development has not been reported; however, Col2-Cre-induced deletion of c-Jun, one of the established JNK substrates, was previously reported to result in a scoliotic phenotype [10]. c-Jun is a major component of the AP-1 transcription factor complex that

plays a role in transcriptional regulation of numerous genes [9]. Knocking out c-Jun in collagen-2–expressing cells resulted in a mouse with abnormalities of the axial skeleton, including scoliosis, thought to be due to increased apoptosis in notochordal cells resulting in a decreased size of the nucleus pulposus in the intervertebral discs [10]. Here, we performed an extensive pathological analysis of the development of the spine, including the vertebral bodies and intervertebral discs, in mice with dKO of *JNK1* and *JNK2* to better understand the role of JNK signaling in spinal development and the pathogenesis of congenital scoliosis.

Materials and Methods

Mice

C57BL/6J mice harboring floxed *JNK1* alleles (*JNK1* $^{fl/fl}$) were a generous gift from Dr. Roger J. Davis at University of Massachusetts Medical School [11]. C57BL/6J *JNK2* conventional KO mice (*JNK2* $^{-/-}$) were obtained from the Jackson Laboratory (Bar Harbor, ME) (stock # 004321). *Col2a1-Cre* (*Col2-Cre*) mice were a generous gift from Dr. Di Chen at Rush University Medical Center (Chicago, IL). The mouse colonies were maintained in a standard specific pathogen-free facility at University of North Carolina at Chapel Hill. Animals had access to water and food ad libitum. All animal experiments were approved by the UNC Animal Care and Use Committee and followed the recommendations from the Guide for the Care and Use of Laboratory Animals of the National Institutes of Health.

The C57BL/6J *JNK1* $^{fl/fl}$ mice were crossed with *JNK2* $^{-/-}$ mice to obtain C57BL/6J *JNK1* $^{fl/+}$ /*JNK2* $^{+/-}$ mice. The C57BL/6J *JNK1* $^{fl/+}$ / *JNK2* $^{+/-}$ mice were then crossed with *Col2-Cre* mice to obtain *JNK1* $^{fl/+}$ *Col2-Cre*/*JNK2* $^{-/-}$ mice which were finally crossed with the C57BL/6J

JNK1 $^{fl/fl}$ / *JNK2* $^{-/-}$ to obtain *JNK1* $^{fl/fl}$ *Col2-Cre*/*JNK2* $^{-/-}$ mice (*JNK1/2* dKO mice). The mice were genotyped using PCR protocols for the specific strains found on the Jackson Laboratory website or as previously described by Das et al [11]. The *JNK1/2* dKO mouse phenotype was analyzed at different embryonic (E11.5, E13.5, E15.5, and E17.5) and postnatal (P11, 4-week– and 10-week–old) stages. In addition to age-matched wild-type (WT) mice, the littermates with the following genotypes were used as controls: *JNK1* $^{fl/+}$ *Col2-Cre*/*JNK2* $^{-/-}$ (Het) and *JNK1* $^{fl/fl}$ /*JNK2* $^{-/-}$ ("CTRL") or *JNK1* $^{fl/+}$ /*JNK2* $^{-/-}$ ("CTRL").

To identify *Col2a1* expressing cells, the loxP-stop-loxP *ZsGreen* reporter mice [B6.Cg-*Gt(ROSA)26Sor*$^{tm6(CAG-ZsGreen1)Hze}$/J (stock # 007906; Jackson Laboratory)] were crossed with *Col2-Cre* mice. *ZsGreen1* is expressed following *Cre*-mediated recombination.

MicroCT analysis

Intact mouse carcasses, excluding skin and abdominal and thoracic viscera, were fixed in 10% formalin for 2 days, and stored in PBS until scanned. Mice at four different ages were scanned: 10-week–old *JNK1/2* dKO (n=2) and control littermates (n=2), a 4-week–old *JNK1/2* dKO and a Het control littermate, 6-week–old *JNK1/2* dKO (n=10, 3 males and 7 females) and control littermates (n=7, 3 males and 4 females), and an 11-day–old *JNK1/2* dKO (n=1) and control littermates (n=2).

The 4-week– and 10-week–old samples were scanned in a transverse plane through the axial skeleton at 55kVp, 0.3-second integration time, with a 30µm voxel size in plane and a 30µm slice thickness ("low resolution") using a Scanco µCT 40 (Scanco Medical AG, Basserdorf, Switzerland). In addition, separate scans (15 µm voxel size) were obtained for select ROIs. In the 10-week–old mice, these ROIs included: i) caudal cervical vertebrae, first few thoracic vertebrae, ii) mid-thoracic vertebrae, and iii) caudal lumbar vertebrae to L6-S1

articulation. In the 4-week–old mice, the ROIs included: i) caudal cervical vertebrae through cranial thoracic vertebrae, and ii) caudal lumbar vertebrae through the L6-S1 junction. 3D reconstructions were made of each scan. For the lower resolution scans (30µm), three ROIs were segmented: i) whole skeleton (including appendicular skeleton), ii) axial skeleton (including pelvis), and iii) axial skeleton without ribs and pelvis.

The 11-day–old mice and the 6-week–old mice were prepared and scanned similarly to the 4- and 10-week–old animals except they were scanned with a Scanco µCT 80 at 45kVp, 0.8-second integration time with an 18 µm (for the 11-day–old mice) voxel size or at 70kVp with a 50 µm (for the 6-week–old mice) voxel size. The region of interest (ROI) for scanning extended from the skull through the pelvis, including the first few caudal vertebrae.

The proper thresholds for overall bone density were tested for each scan and each age group and the same thresholds were used throughout the study.

In addition, the magnitude of scoliosis severity were quantified in the 6-week–old group by measuring the Cobb angle [12], which measures the degree of curvature in the spine, in 2D snapshots of the microCT using ImageJ1.48v (National Institute of Mental Health, Bethesda, MD). Although all dKO mice had lumbar scoliosis, some of them also had scoliosis at the level of the thoracic spine, therefore, for simplicity, the Cobb angle was measured only at the level of the lumbar spine in all animals.

Histological assessment of 4-week–old and 10-week–old *JNK1/2* dKO and controls

Tissues were dissected and fixed in formalin, decalcified in Immunocal (StatLab Medical Products, McKinney, TX # 1414-1) for two days (for 4-week–old mice) or 4 days (for 10-week–old mice) and prepared for histological analyses as previously described [13]. In brief, intact spines

were separated from the head and tail and divided into cervical, thoracic, and lumbar/sacral segments. They were embedded using a Leica (Leica Biosystems Inc., Buffalo Grove, IL) embedding unit (HistoCore Arcadia) with 5 µm sections collected throughout the spine using a Leica microtome (RM2235). Due to dKO spinal torsion, which made the embedding in a single plane difficult, the dKO vertebral columns were embedded and sectioned first and then the control samples were oriented to match the plane of the dKO, some in the sagittal plane and others in the coronal plane. The sternum was embedded/sectioned in the coronal plane for all genotypes. Proximal tail intervertebral disc (IVD) width, annulus fibrosus (AF) and nucleus pulposus (NP) width, and height and vertebral growth plate (GP) structures were measured using Image J1.48v.

Stifle (knee) joints were collected from all genotypes. Knee joints were embedded and sectioned (5 µm) in the coronal orientation. From each knee, one slide from a specific location in the mid-coronal region was used for safranin O/fast green staining, as previously described [13, 14] with slight modifications. The location was identified by the shape of the menisci (which shows the meniscus finishing into a pointed tip and completely separated from the center of the joint) [14]. The slides were re-hydrated, stained in fast green (fast green FCF, Sigma-Aldrich, St. Louis, MO, #F 7252) solution (0.02%) for 25 min, washed in 1% acetic acid, stained in safranin O (Sigma-Aldrich, #S8884) solution (1.5%) for 30 min, dehydrated, and mounted with Permount (Fisher Scientific, Waltham, MA, #SP15-100). Images were taken using an Olympus (Waltham, MA) microscope (BX60), camera (DP73), and software (cellSens v1.16). Measurements of 10-week–old joint width (from one femoral condyle to the other), GP, articular cartilage (AC), and subchondral bone (SB) thickness, were analyzed using Image J1.48v.

Histologic assessment of *JNK1/2* dKO and controls at different embryonic stages

Embryos were collected from timed-pregnant mice at E11.5, E 13.5, E15.5, and E17.5. At E11.5, whole embryos were fixed in formalin for 2 days and embedded/sectioned (5 µm) in sagittal orientation. At E13.5, whole embryos (without the head) were fixed in formalin for 2 days and embedded/sectioned (5 µm) in sagittal orientation. At E15.5 and E17.5, whole embryos were fixed in formalin for 2 days, then the entire spine, sternum, and tibiae were collected and embedded/sectioned (5 µm) in sagittal (spine) and coronal (tibia, sternum) orientation. Tissues were stained with Hematoxylin (Harris Hematoxylin, Sigma-Aldrich, #HHS16-500 mL) and Eosin (Alcoholic Eosin Y 515, Leica Biosystems/Surgipath, #3801615) (H&E) and safranin O/fast green as detailed above. Measurements of E17.5 spinal structures (GP, NP, and AF) were taken at the level of two thoracic segments (T10-T11 and T11-T12) using Image J 1.48v and they were reported as an average (AVG).

Alcian blue/Alizarin red skeletal stain

Mice were sacrificed at 3.5 to 4 (n=4; 2 CTRL/Het, 2dKO) and 10 weeks (n=2; 1CTRL/Het, 1 dKO) of age and embryos at E17.5 (n=6; 3dKO, 3CTRL) and skin and organs were removed prior to fixation in 95 % ethanol overnight and then in acetone overnight, as previously described [15]. Tissues were stained with Alcian blue solution (0.03% in 80% EtOH and 20% glacial acetic acid) for 3 days (4- and 10-week–old animals) or for 1 day (embryos). The tissues were destained in 70 % ethanol for one hour and in 95% ethanol overnight. The ethanol was then replaced with 1% KOH clearing solution for four hours and then stained with Alizarin red solution (0.005% in 1% KOH) for 2 days (4 and 10 week-old animals) or 3 hours (embryos) followed by incubation in 1% KOH until the soft tissue disintegrated (1-2one to two weeks, with daily monitoring). The mice were stored long-term in 70% ethanol/glycerol (1:1). Specific areas

of interest and whole body embryo skeletons were captured using an Olympus SZX16 research high-class stereo microscope.

Picrosirius red stain

Spine sections of 3.5 to 4-week–old (n=6; 3dKO, 3CTRL) and 10-week–old (n=6; 3dKO, 3CTRL) mice and E15.5 (n=6; 3dKO, 3CTRL) and E17.5 (n=6; 3dKO, 3CTRL) embryos were also stained with picrosirius red stain following the manufacturer's recommendations (Polysciences, Inc, Warrington, PA, #24901-250). Briefly the slides were hydrated and incubated with Phosphomolybdic acid (solution A) for 2 minutes, rinsed in dH_2O, and incubated with Picrosirius red F3BA stain for 60 minutes, 0.1N HCl for 2 minutes, and then the slides were dehydrated and mounted. The slides were visualized under polarizing light using a Nikon (Melville, NY) 2000E microscope.

Immunohistochemistry

Immunohistochemistry was performed as previously described [16], with minor modifications. Sections were incubated in 3% H_2O_2 for 15 min at room temperature, followed by incubation in 0.1% Triton X-100 for 15 min at RT (for the following antibodies: collagen type X, Runx2, p57, PCNA, and Sox-9) or by incubation in 10 mM sodium citrate solution (pH 6.0) for 30 min at 97 °C (for the following antibodies: ZsGreen, , p-cJun, p-Smad2, p-Smad1,5,8), or without antigen retrieval (JNK1/2). Sections were then washed in PBS and blocked with 5% goat serum (for Sox-9, ZsGreen, p-JNK1/2, p-cJun, p-Smad2, p-Smad1,5,8) or Dako protein block (Agilent, Santa Clara, CA, #XO909- for collagen type X, Runx2, p57, PCNA). Sections were incubated with anti-Sox9 (R&D, Minneapolis, MN, AF3075, 1:300 dilution of the original stock), ZsGreen (Clontech/Takara Mountain View, CA #632474, 1:200), collagen type X (Abcam, Cambridge,

MA, #ab58632, 1:500), p57 (Santa Cruz, Dallas, TX #sc-56341, 1:200), Runx2 (Santa Cruz, #sc-390351,1:100), p-cJun (Cell Signaling Technology, Danvers, MA, #3270S, 1:100), JNK1/2 (BD Pharmingen, San Diego, CA, #554285, 1:100), p-Smad2 (Cell Signaling Technology, #3108T, 1:100) and -p-Smad1,5,8 (9) (Cell Signaling Technology, #13820, 1:100) primary antibodies over night at 4 °C. For the Sox-9 IHC a rabbit anti-goat horseradish peroxidase (HRP)-conjugated secondary antibody (Abcam, #ab97100), which was visualized using DAB (Agilent, Dako Liquid DAB+ Substrate Chromogen System #K3468), was used. For the rest of the antibodies the UltraVision LP Large Volume Detection System AP Polymer (Agilent, Dako EnVision+ System- HRP Labelled Polymer Anti-Rabbit #K4002 or anti-mouse #K4000) was used, instead of the secondary antibody, followed by DAB (~5 min.) Sections were then counterstained with methyl green for 5 min, washed, and mounted. Pictures and image processing were performed as described above.

Protein extraction and immunoblotting

Protein was extracted from femoral epiphysis cartilage (femoral caps), muscle, and IVD from 4- to 6-week–old dKO and control mice. Femoral caps were removed from the femoral head with forceps. The thoracic vertebral column IVDs were separated from the adjacent tissues at the level of the growth plate (GP), therefore the samples contained AF, NP, CEP, and a portion of the GP. The tissues were lyzed in 150 µL lysis buffer (Cell Signaling Technology #9803) supplemented with PMSF (Sigma #93482) and HALT phosphatase inhibitor (Thermo Fisher Scientific, #78428). The tissue was homogenized using ceramic bead tubes (Qiagen/MOBIO Laboratories, Germantown, MD; 1.4-mm beads) and a Precellys homogenization device (Bertin Technologies, Rockville, MD) for three 40-s cycles at 6,500 rpm. After homogenization, samples were centrifuged for 5 min at 13,000 rpm to pellet insoluble material and then the protein was

prepared for immunoblotting as previously described [16, 17]. The immunoblots were stained with a total protein stain (Thermo Fisher Scientific, #24580 Pierce reversible protein stain) to check for equal protein loading. The immunoblots were probed with an antibody against JNK1and 2 (BD Pharmingen, San Diego, CA, #554285) at 4 ^{0}C overnight and visualized by chemiluminescence.

TUNEL assay

E11.5 and E13.5 sections were assessed for apoptosis using the ApopTag Plus Peroxidase In Situ Apoptosis Detection kit (Millipore, Burlington, MA, #S7101), by following the manufacturer's recommendations. The slides were counterstained with Methyl green. Pictures and image processing were performed as described above. The TUNEL positive cells (brown stain) at E11.5 were counted using Image J in the condensations representing future IVD, inside the notochord and perinotochordal sclerotome (in both condensed and non-condensed areas). The cell counts in the notochord region were normalized to the length of the notochord within the field of view.

Statistical analysis

Unless otherwise mentioned, the data were analyzed using GraphPad Prism 7.03 (La Jolla, CA). For the vertebral body and IVD embryo measurement, where only CTRL and dKO groups were compared, two-tailed unpaired Student's *t*-test was used. For the tail IVD and other measurements comparing CTRL, WT, and dKO, one-way ANOVA followed by Tukey's multiple comparisons post-hoc test was used. A *P*-value of ≤ 0.05 was considered statistically significant.

Results

Col2-Cre recombinase expression pattern in the skeleton

The same strain of *Col2-Cre* mice used to generate the *JNK1/2* dKO, was crossed with ZsGreen reporter mice to identify Cre expressing cells in tissues containing collagen type 2. Immunohistochemistry was performed with an antibody against ZsGreen and positive cells were observed in developing long bones (Fig.1 A, D, G, J), vertebral column, vertebral body (VB) and IVD tissues including the nucleus pulposus, inner annulus fibrosus, and the cartilage end plate (CEP) (Fig.1 B, E, H, K), and sternum and ribs (Fig.1 C, F, I, L).

Severe scoliotic phenotype in the *JNK1/2* dKO mice

Around weaning age, the *JNK1/2* dKO mice could be easily identified by abnormal gait, a protuberant abdomen, and an upward tail orientation. All other genotypes, including WT and littermates with the following genotypes: *JNK1* $^{fl/+}$ *Col2-Cre*/*JNK2* $^{-/-}$ (Het) and *JNK1* $^{fl/fl}$ /*JNK2* $^{-/-}$ ("CTRL") or *JNK1* $^{fl/+}$ /*JNK2* $^{-/-}$ ("CTRL") appeared to develop normally. Overall, the dKO mice were smaller than the control genotypes (Fig.2 A, B, E, I), but the most affected region seemed to be the axial skeleton (Fig.2). At around 10 weeks of age, the mice had to be euthanized due to urinary retention and paraphimosis. In total, 222 mice were analyzed for this study and all of the 37 dKO mice analyzed manifested the skeletal phenotype (both males and females) whereas none of the other genotypes exhibited the phenotype (Table 1).

The skeletal phenotype was associated with vertebral fusions as seen both by microCT and Alcian blue/Alizarin red staining (Fig.2). MicroCT analysis showed that most of the vertebrae were fused in the dKO, and no spaces were observed in the area where the IVD should be located (Fig.2 A-D). In the 10-week–old dKO animals, gaps were noticed between vertebrae as seen in the dorsal view (Fig.2 B). In 4-week–old dKO mice, the ectopic ossification and resulting abnormal curvature of the spine was mostly localized to the caudal thoracic and lumbar spine. Fusions associated with the posterior elements and vertebral bodies could be detected in

both the lumbar and thoracic spine (Fig.2 A). Ectopic ossifications were associated with numerous structures of the vertebrae, including the transverse and spinous processes (Fig.2 A-D). Skeletal preps stained with Alcian blue/Alizarin red showed that the vertebral body fusion at the level of the dKO IVDs was more cartilaginous in nature in the thoracic spine and more boney in the lumbar spine (Fig.2 F, G). Numerous osteophytes were present in the dKO at the level of the vertebral body as well, as seen by lack of the normal vertebral contour (Fig.2 C). Measuring scoliosis severity using the Cobb angle in the 6-week–old group revealed that while all the analyzed dKO mice showed significant scoliosis (lowest angle 40 degrees, which in humans is considered moderate scoliosis that requires therapy[18]) there was some variability in the phenotype with angles ranging from 40 to 92 degrees. Findings were similar in the male and female groups (Fig.2 J).

JNK 1 and 2 levels were assessed by immunoblotting using femoral head cartilage (FC), muscle, and IVD with an antibody that recognizes both JNK1 and 2, and both major and minor isoforms of these proteins. Both JNK1 and 2 were very low in dKO FC and IVD, though not completely absent, probably due to protein contamination from other tissue types during dissection and the fact that Col2-Cre would not target all cells in the outer AF in the dKO mice. In dKO muscle tissues, the two JNK2 isoforms (major and minor) were absent whereas JNK1 was still present, as expected, since Col2-Cre would not be expressed in muscle (Fig.3 A). The expression of JNK1 and 2 was analyzed by immunohistochemistry in E 17.5 embryo IVDs, when the skeletal phenotype was just starting to manifest. In the WT E17.5 embryos, the two proteins were expressed in IVD, VB, and the connective tissue surrounding them (Fig.3 B,E). At the level of the IVD, JNK1 and 2 were expressed both in the AF (especially in the inner AF) and in the NP. In the IVDs and VB of $JNK1^{fl/fl}/JNK2^{-/-}$ embryos (Fig.3 C, F), fewer cells express JNK1/2 in

the IVD (due to loss of JNK2 in these mice) and the expression is virtually absent in the dKO (Fig.3 D, G), while both genotypes still show expression of the two proteins in the surrounding connective tissue.

Fusion of vertebral processes is an early event in *JNK1/2* dKO mice

Since the vertebral fusions were already very severe in the dKO mice at 4 weeks of age, making it impossible to assess the initiating changes, the phenotype was analyzed at postnatal day11 (P11) by microCT. At this stage, the dKO mice showed vertebral fusions in the transverse and spinous processes with the most advanced lesions localized to the lumbar spine (Fig.4 A-C). Vertebral fusions were also present in the thoracic spine, especially caudal to T6 (Fig.4 A). The transverse processes seemed to fuse in an asymmetrical fashion, for example, starting at L5 and continuing to T12 on the right side, while starting at L3 on the left side (Fig.4 A, B). Calcified IVD tissues were noted between vertebrae (Fig.4 C).

The presence of fused vertebrae before weaning age suggested that this process started much earlier, probably during embryonic development. The skeletons of E17.5 mutants and controls were therefore investigated, using the Alcian blue/Alizarin red stain (Fig.4 D). Fusions dorsally, at the level of the vertebral arches (Fig.4 E) and an abnormal shape of the primary ossification centers of these arches was noticed (Fig.4 F).

IVD tissues replaced by cartilage and bone in *JNK1/2* dKO mice

The IVDs in the regions of fusion were further studied. The IVD is composed of three compartments: the NP, a gel-like structure, rich in proteoglycans; AF, a fibrocartilaginous tissue that surrounds the NP; and the CEP, which separates the NP from the adjacent vertebral bodies [19]. The tissues forming the IVD are not only structurally distinct but they also derive from

different embryonic cell populations. The NP is derived from the notochord, whereas the AF, CEP, and vertebral bodies develop from the condensed and non-condensed regions, respectively, of the perinotochordal tube, which derives from the ventral sclerotome[10, 19]. The vertebral bodies develop through the process of endochondral ossification in which the cartilage anlagen will be replaced by bone tissue [10, 19]. The other vertebral structures, such as neural arches, derive from the lateral sclerotome [20, 21]. Dysregulation of these tightly regulated processes could lead to defects in IVD development and function, including abnormal bone formation around and within these tissues and abnormal fusions of adjacent vertebrae that could ultimately lead to diseases such as scoliosis.

Safranin O/fast green staining of spinal segments from 4-week–old mice showed an overall reduction in NP size. The AF was replaced by chondrocyte-like cells in the dKO mice (Fig.5 A-P). In dKO mice, the typical lamellar structure of the AF was completely absent (Fig.5 D, H, L, P). At 10 weeks of age most of the area previously occupied by the AF and NP was replaced by both bone and cartilage tissues in the IVDs of the lumbar (Fig.5 T, X) and caudal thoracic spine (not shown), suggesting that an abnormal endochondral ossification process was taking place within the IVD. In the proximal thoracic spine (approximately cranial to T9), the IVD was replaced by proteoglycan-rich cartilaginous tissue which extended beyond the disc and appeared to connect the distal and proximal growth plates of adjacent vertebral bodies (not shown but similar to the 4-week–old proximal thoracic spine (Fig.5 D)).

In the annulus fibrosus the lamellar organization of ECM also appeared to be lost in dKO mice. To assess the organization of the collagen matrix, IVD tissue sections were stained using picrosirius red staining and visualized by polarized light (Fig.6 A-H). In both the 10- (not shown) and 4-week–old dKO mice (Fig.6D, H) the organization of collagen-rich laminae was absent,

when compared to the other genotype controls which showed the concentrically organized laminae that run obliquely from one vertebra to the other (Fig.6 A-C, E-G).

Hypertrophic chondrocyte markers localized to the area of annulus fibrous in the 4- and 10-week–old dKO mice

Since the histological sections of the intact spine of adult dKO mice showed a replacement of the intervertebral disc structures (AF and NP) by cartilage and bone tissues (Fig. 5), the phenotype of these IVD cells were assessed by immunohistochemistry with markers for chondrocytes, hypertrophic chondrocytes, and osteoblasts. Very few of the AF or NP cells were proliferating, such as a few outer AF cells in the controls and dKO, and in the areas of new bone formation in the dKO, as shown by the PCNA staining (Fig.7 E, J). There was no statistically significant difference between the genotypes (4- and 10-week–old, CTRL/Het, n=5, dKO, n=5) regarding the number of PCNA positive cells located between the NP and the outer edge of AF (Fig. S1 N). Most cells within the region of IVD in the dKO mice expressed markers of chondrocytes (SOX-9, Supplemental Fig. S1 G-I) and hypertrophic chondrocytes, such as collagen type X (Fig.7 B, G) and p57 (Fig.7 C,H) as well as Runx2 (Fig.7 D,I), a marker of hypertrophic chondrocytes/osteoblasts.

To further investigate the phenotype of these cells at the time when the alterations were first noticed in AF development and to identify a possible initiating event, the above-mentioned markers in E17.5 dKO and control vertebral columns were analyzed. The larger chondrocyte-like cells taking over the AF in the dKO expressed chondrocyte markers (Supplemental Fig. S1K) and markers of proliferation (Supplemental Fig. S1M) but so did the AF cells in the control genotypes (Supplemental Fig. S1J and L).

Normal notochord development, abnormal organization of the annulus fibrosus, and fusion of vertebral posterior processes in the dKO embryos

Since changes in spinal development were seen at E17.5, the phenotype of the dKO and control mice was analyzed in further detail by histology at E11.5, E13.5, E15.5, and E17.5. H&E–stained sections of embryos at E11.5 (Fig.8 A-C) and E13.5 (Fig.8 D-F) showed what appeared to be normal development of the notochord in all genotypes. At E11.5, in serial sections, the notochord was observed throughout the developing spine, from cranial to caudal sites. In addition, the normal alternation between condensed (the site where the future IVD will form-intervertebral regions) and non-condensed (where the vertebral body will form-vertebral regions) areas was observed in the perinotochordal sclerotome in all genotypes (Fig8 A-C). Similarly, at E13.5 the notochord was present and showed similar characteristics in all genotypes, including increased cell density in the site of the future NP. At this stage the vertebral body condensations could be observed as well as alternating intervertebral regions, and the patterning seemed similar between all genotypes (Fig.8 D-F).

H&E–stained sections of the vertebral column at E15.5 (Fig.9 A-F) and E17.5 (Fig.9 G-L) following segmentation of the IVDs revealed an abnormal organization of the AF in the dKO mice. In contrast to control genotypes where AF cells were aligned between lamellae (Fig.9 A, B, D, E) starting at E 15.5 the AF of dKO mice was populated by larger, chondrocyte-like cells (Fig.9 C, F) which showed an altered alignment of the collagen fibers in the laminae. Similar results were found at E 17.5 (Fig 9I, L). In addition, fusions of the caudal vertebral processes were detected at E15.5 (not shown) and E17.5 stages in the dKO (Fig.9 M-O). Measurements of skeletal structures in the dKO mice at E17.5 using Image J in H&E sections, revealed decreased vertebral GP length (Fig.10 A) and increased AF width both for the dorsal (not shown) and

ventral regions (Fig.10 B) compared to CTRL. The NP seemed to be organized normally at E15.5 and E17.5, and measurements of NP height (not shown) and width (Fig.10 C) at E 17.5 were not statistically different between the groups.

Due to severe abnormality of the IVD in the cervical, thoracic, and lumbar vertebral column in the older animals, differences in IVD size were analyzed at the level of the cranial tail (caudal) vertebrae in 4-week–old dKO and control mice (WT and CTRL). The width of the IVD (Fig.10 D) and the height (Fig.10 E) and width (Fig.10 F) of the NP were decreased in the dKO mice compared to control genotypes.

Presence of fusions at the level of sternum

Sternum, another component of the axial skeleton, was also affected in the dKO mice. The sternum and the sternal ribs derive from the lateral plate mesoderm [22] and so they have a different developmental origin than the rest of the axial skeleton, but cells within demonstrate a fibrocartilage phenotype at skeletal maturity that shares common features such as ECM composition with the annulus fibrosus. Alcian blue/Alizarin red staining of these tissues showed fusions of the sternebrae in the 10-week–old dKO mice (Fig.11 A,B) and Saf O/FG-stained sections showed altered organization of the fibrocartilaginous tissue separating the sternebrae (Fig.11 C, D). These changes were similar to those noted in the annulus fibrosus, with an increased production of a cartilaginous tissue rich in proteoglycans. The separation between ribs and sternum at the sterno-costal joint was not well defined in the dKO mice compared to controls (yellow circles). There was also an enlargement of the GP in the sternebrae (Fig.11 C, D).

Analysis of embryonic tibia and 4- and 10-week–old knee joints

There was no significant difference in the tibia length (not shown) or the length of the GP (Fig.12 A-D) or height of mineralized regions (Fig.12 A-D) among the genotypes at E17.5; however, a trend toward decreased values in the dKO was not seen. The tibial growth plate (GP) appeared to be normally organized.

At both four (not shown) and 10 weeks of age, the articular cartilage of the knee joint did not show any obvious abnormalities in the dKO (Fig.12 E-G). Measurements of the tibia GP length did not show any significant differences among genotypes (not shown). The articular cartilage (AC) thickness (Fig.12 I), the width of the knee joint at the level of the femoral condyles (Fig.12 H), and the height of the tibial plateau [epiphysis + metaphysis: AC+GP+ subchondral bone (SB)] (Fig.12 J) were decreased in the dKO.

Decreased c-Jun phosphorylation in the mutant AF and NP

While exploring different mechanisms that could explain the phenotype of the *JNK1/2* dKO mice and knowing that *c-Jun* (a member of the JNK pathway) KO has a similar skeletal phenotype, it was investigated whether c-Jun phosphorylation was affected in the *JNK1/2* mutants. As expected, since c-Jun is phosphorylated primarily by JNK, there was an absence of immunostaining for phosphorylated (phospho) c-Jun in the NP and decreased staining in the AF and the vertebral body of the dKO mice at E17.5 (Fig 13 A, B) with no difference in the immunostaining among genotypes in tissues such as the spinal cord and other tissues adjacent to the vertebral column. The strongest phospho-cJun signal was noticed in the NP of the control groups.

The levels of phospho-c-Jun were also reduced in the tibiae of dKO mice compared to control which exhibited phospho-cJun staining in the prehypertrophic zone of the growth plate

(data not shown). Although the overall phospho-c-Jun levels were very low, a few positive cells were observed in the 10-week–old control IVD, mostly in the outer AF, whereas the dKO had no staining in this region (Suppl.Fig. 1A-C). At 10 weeks, phospho-c-Jun was absent from NP in all genotypes (Suppl. Fig. 1A-C), whereas at four weeks of age, there was still some signal in the control NP, but it was absent in the dKO NP (not shown).

In the case of the *c-Jun* KO, the main mechanism suggested for the reported phenotype was increased apoptosis of the notochord. Since decreased c-Jun phosphorylation was observed in the *JNK1/2* dKO, the differences in apoptosis between the *JNK1/2* dKO and controls were further explored. Unlike the report of the *c-Jun* KO [10] , a difference in TUNEL positive cells between the controls and the *JNK1/2* dKO was not seen (Fig.12 E-J).

Analysis of TGF β/BMP signaling in tissues isolated from dKO and control mice

Due to the increased formation of cartilage and bone tissues at the level of annulus fibrosus, a process resembling endochondral ossification, pathways that could increase tissue turnover and stimulate this process were investigated. TGF β/BMP signaling is essential for cartilage and bone formation and these pathways have also been suggested to contribute to scoliosis in the *filamin B* KO mouse. In addition, TGFβ was previously reported to be up-regulated in cells with decreased JNK activity, such as MEFs isolated from *JNK1/2* dKO [23]. The levels of phospho-Smad2, as a marker of TGFβ activity, and phospho-Smad1/5/8, as a marker of BMP activity, was analyzed by immunoblotting and IHC in cartilage, muscle, and IVD isolated from dKO and control genotypes. At four and 10 weeks of age, phospho-Smad 1/5/8 was present mostly in the NP region and fewer positive cells were present in the dKO mice, most likely due to the small size of the NP in these mice (Supplemental Fig. S1D-F). However, even when the NP was present in the dKOs, the phospho-Smad1,5,8 immunostaining was either very weak or absent (not shown).

Phospho-Smad2 was present in the AF, NP, and some parts of the vertebral growth plate (not shown) and no obvious differences were seen in the number of phospho-Smad2 positive cells among the genotypes.

Discussion

Scoliosis affects millions of individuals worldwide and frequently the cause remains unknown. There are different types of scoliosis, depending on the timing of the clinical presentation. In congenital scoliosis the deformation of the spine is already present at birth due to vertebral abnormalities during development, while most cases of scoliosis present after birth and have no known cause and so are considered idiopathic scoliosis [24]. In the present study of *JNK1/2* dKO mice, a congenital scoliotic phenotype with extensive and progressive fusion of the vertebrae that began during development, prior to embryonic day 15.5 was noted. The vertebral fusion appeared to be due to ectopic endochondral ossification occurring in the AF and around the vertebrae, possibly at the level of the spinal ligaments resulting from abnormal differentiation of cells to hypertrophic chondrocytes. The NP was also affected but this appeared to be secondary to changes in the surrounding AF. The sternum exhibited abnormal fusion with the ribs at the sternocostal joints, whereas the notochord was not affected. The *JNK1/2* dKO was generated by knockout of *JNK1* induced using Col2-cre in mice with a *JNK2* deletion. Although Col2 is expressed in the appendicular joints, unlike the findings in the spine and sternum, they exhibited no or minimal changes suggesting a more important role for JNK1/2 signaling in the development and maintenance of the axial skeleton. Since the phenotype was present only when both *JNK1* and *JNK2* (but not *JNK3*) were deleted, the results suggest redundant functions for *JNK1* and *JNK2* genes in spine development whereas the presence of JNK3 was not sufficient to prevent the development of the scoliosis phenotype.

The AF, as well as the sternebrae, are fibrocartilaginous tissues that contain both type I and type II collagen with type II collagen being more predominant in the inner region than the outer region of the annulus [25]. Type II collagen is also found in the NP. It was in these regions where the cells exhibited features consistent with chondrocyte hypertrophy, suggesting that JNK signaling in *Col2*-expressing cells in these tissues inhibits hypertrophic differentiation and subsequent endochondral bone formation. A similar mechanism occurring in the vertebral growth plates may be responsible for the reduced growth plate thickness.

There are some similarities of the scoliotic phenotype seen here to those seen with *Col2*-cre–mediated deletion of *c-Jun* [10] and a germ-line mutation in filamin B [26, 27]. Because JNK phosphorylates and activates c-Jun, it is not surprising that a similar scoliotic phenotype with vertebral fusion and abnormalities in the sternum and intervertebral discs were seen in both the *c-Jun* and *JNK1/2* dKOs. The spinal phenotype seen with loss of c-Jun was attributed to increased apoptosis in notochordal cells resulting in IVD hypocellularity. Unlike in the *c-Jun* KO, differences in TUNEL staining, as a measure of apoptosis, were no seen in the E11.5 *JNK1/2* dKO at the level of the notochord or the sclerotome. In addition, the *JNK1/2* dKO phenotype seemed to be more severe than the *c-Jun* KO phenotype in terms of the degree of vertebral fusion, suggesting that alteration in c-Jun activity might only partly explain the *JNK1/2* dKO phenotype.

The spine phenotype of the *JNK1/2* dKO mice also resembles the phenotype of the filamin B KO mouse that exhibited vertebral and sternal fusions and loss of the IVD associated with hypertrophic cells in the AF [26, 27]. Filamin B is one of the only few genes that have been associated with congenital scoliosis. The filamin B KO mouse was used to model the human disease spondylocarpotarsal synostosis, a form of severe scoliosis presenting early in life that is

accompanied by fusion of carpal and tarsal bones[18]. The ossification and fusion of the posterior vertebral processes in the *JNK1/2* dKO mice resembles the unsegmented bar noted in the posterior processes in a 13-year–old girl with spondylocarpotarsal synostosis syndrome [28] and in the filamin B KO mice [26, 27]. However, unlike the filamin B KO mouse and spondylocarpotarsal synostosis syndrome, the presence of tarsal or carpal fusions was not seen in these mice (Supplemental Fig. S2).

Neither the filamin B nor the *c*-Jun KO mice presented a skeletal phenotype in the long bones [10, 26]. Although some changes were seen in AC thickness and width of the femur in the 10-week–old *JNK1/2* dKO mice, there were no obvious GP abnormalities in the *JNK1/2* dKO embryos. These findings may be explained by a possible decreased nutritional intake as a result of severe scoliosis and the subsequent affected mobility in these mice and the increased caloric expenditure as a result of increased respiration effort due to decreased chest volume (thoracic insufficiency syndrome [29]). Currently, the differences between the axial and the appendicular skeleton phenotype cannot be explained. Perhaps JNK1 and 2 are essential for specific steps in the IVD and vertebral column development and not for the endochondral ossification process at the level of the long bone growth plate.

The role of JNK and filamin B in the development of the spine may be connected at the level of the TGFβ/BMP signaling pathways that regulate bone formation. TGFβ/BMP signaling was shown to be increased in the annulus fibrosus of filamin B KO mice [27] and it has been shown that TGFβ is up-regulated in *JNK1/2* dKO fibroblasts [23]. Evidence for increased phosphorylation of the TGFβ target Smad2 was not found; however, phosphorylation of the BMP target Smad1, 5, 8 appeared to be decreased rather than increased in the *JNK1/2* dKOs, particularly in the NP. Further studies are needed to determine the mechanism by which loss of JNK signaling results in

the abnormal hypertrophic differentiation and subsequent endochondral bone formation seen in the *JNK1/2* dKO IVDs and vertebral processes.

The etiology of congenital scoliosis in humans is multifactorial with genetic and environmental factors playing a role. Vertebral anomalies are classified as either failure of proper vertebral formation, failure of appropriate segmentation, or mixed. Similar to the findings in the *JNK1/2* dKO mice, these changes occur early in the development of the human embryo, prior to complete differentiation of the vertebral body or IVD [30]. Failure of segmentation, once considered to be a metaplastic change of the annulus fibrosis causing tethering between vertebral bodies, is now thought to be a result of chondrification of mesenchymal precursors (instead of the typical differentiation into fibroblasts) which lead to congenital fusions rather than IVD development [31]. This pathophysiology shares many of the same characteristics with the present model of murine scoliosis, including the embryonic origin and the early chondrification of the periphery of the IVD leading to congenital fusion. In both mouse and human forms of the disease, any small asymmetry in the presence of a peripheral fusion will lead to differential growth in the developing spine, with the tethered region becoming the concavity of a deformity as the rest of the vertebral column "crankshafts" around the tether. In contrast to the JNK1/2 dKO mice, humans with this condition have a less severe phenotype and do not typically develop an osseous fusion between the majority of vertebra unless as a result of degenerative disease much later in life.

The *JNK1/2* dKO is a potential model to study congenital scoliosis and vertebral fusions, especially since 100% of the dKO mice exhibited the axial skeletal phenotype. Further assessment should be done to identify members of the JNK pathway, either upstream or downstream of JNK1/2, as possible candidate genes for human congenital scoliosis.

Acknowledgements

We thank Dr. Paul Maddox (UNC-Chapel Hill, Biology Department) and the Hooker Imaging Core at UNC-Chapel Hill for help with polarizing light microscopy, Dr. Oscar Alvarez Garcia (The Scripps Research Institute) for helpful discussion regarding IVD development, Zhao Yiwen (UNC-Chapel Hill) and Helen Willcockson (UNC-Chapel Hill) for help with histology and imaging, Dr. Roger Davis for providing the *JNK1*$^{fl/fl}$ mice, and Dr. Di Chen for providing *Col2a1-Cre* mice.

References

[1] Beier F, Loeser RF: Biology and pathology of Rho GTPase, PI-3 kinase-Akt, and MAP kinase signaling pathways in chondrocytes. J Cell Biochem 2010, 110:573-80.
[2] Bobick BE, Kulyk WM: Regulation of cartilage formation and maturation by mitogen-activated protein kinase signaling. Birth Defects Res C Embryo Today 2008, 84:131-54.
[3] Clancy R, Rediske J, Koehne C, Stoyanovsky D, Amin A, Attur M, Iyama K, Abramson SB: Activation of stress-activated protein kinase in osteoarthritic cartilage: evidence for nitric oxide dependence. Osteoarthritis Cartilage 2001, 9:294-9.
[4] Loeser RF, Erickson EA, Long DL: Mitogen-activated protein kinases as therapeutic targets in osteoarthritis. Curr Opin Rheumatol 2008, 20:581-6.
[5] Wood ST, Long DL, Reisz JA, Yammani RR, Burke EA, Klomsiri C, Poole LB, Furdui CM, Loeser RF: Cysteine-mediated redox regulation of cell signaling in chondrocytes stimulated with fibronectin fragments. Arthritis Rheumatol 2016, 68:117-26.
[6] Fanning PJ, Emkey G, Smith RJ, Grodzinsky AJ, Szasz N, Trippel SB: Mechanical regulation of mitogen-activated protein kinase signaling in articular cartilage. J Biol Chem 2003, 278:50940-8.
[7] Kyriakis JM, Avruch J: Mammalian mitogen-activated protein kinase signal transduction pathways activated by stress and inflammation. Physiol Rev 2001, 81:807-69.
[8] Kuan CY, Yang DD, Samanta Roy DR, Davis RJ, Rakic P, Flavell RA: The Jnk1 and Jnk2 protein kinases are required for regional specific apoptosis during early brain development. Neuron 1999, 22:667-76.
[9] Bode AM, Dong Z: The functional contrariety of JNK. Mol Carcinog 2007, 46:591-8.
[10] Behrens A, Haigh J, Mechta-Grigoriou F, Nagy A, Yaniv M, Wagner EF: Impaired intervertebral disc formation in the absence of Jun. Development 2003, 130:103-9.
[11] Das M, Jiang F, Sluss HK, Zhang C, Shokat KM, Flavell RA, Davis RJ: Suppression of p53-dependent senescence by the JNK signal transduction pathway. Proc Natl Acad Sci U S A 2007, 104:15759-64.
[12] Tauchi R, Tsuji T, Cahill PJ, Flynn JM, Flynn JM, Glotzbecker M, El-Hawary R, Heflin JA, Imagama S, Joshi AP, Nohara A, Ramirez N, Roye DP, Jr., Saito T, Sawyer JR, Smith JT, Kawakami N: Reliability analysis of Cobb angle measurements of congenital scoliosis using X-ray and 3D-CT images. Eur J Orthop Surg Traumatol 2016, 26:53-7.

[13] Ulici V, Kelley KL, Azcarate-Peril MA, Cleveland RJ, Sartor RB, Schwartz TA, Loeser RF: Osteoarthritis induced by destabilization of the medial meniscus is reduced in germ-free mice. Osteoarthritis Cartilage 2018.
[14] McNulty MA, Loeser RF, Davey C, Callahan MF, Ferguson CM, Carlson CS: A comprehensive histological assessment of osteoarthritis lesions in mice. Cartilage 2011, 2:354-63.
[15] Rigueur D, Lyons KM: Whole-mount skeletal staining. Methods Mol Biol 2014, 1130:113-21.
[16] Collins JA, Wood ST, Nelson KJ, Rowe MA, Carlson CS, Chubinskaya S, Poole LB, Furdui CM, Loeser RF: Oxidative stress promotes peroxiredoxin hyperoxidation and attenuates pro-survival signaling in aging chondrocytes. J Biol Chem 2016, 291:6641-54.
[17] Del Carlo M, Jr., Loeser RF: Nitric oxide-mediated chondrocyte cell death requires the generation of additional reactive oxygen species. Arthritis Rheum 2002, 46:394-403.
[18] Reamy BV, Slakey JB: Adolescent idiopathic scoliosis: review and current concepts. Am Fam Physician 2001, 64:111-6.
[19] McCann MR, Tamplin OJ, Rossant J, Seguin CA: Tracing notochord-derived cells using a Noto-cre mouse: implications for intervertebral disc development. Dis Model Mech 2012, 5:73-82.
[20] Barrionuevo F, Taketo MM, Scherer G, Kispert A: Sox9 is required for notochord maintenance in mice. Dev Biol 2006, 295:128-40.
[21] Christ B, Wilting J: From somites to vertebral column. Ann Anat 1992, 174:23-32.
[22] McIntyre DC, Rakshit S, Yallowitz AR, Loken L, Jeannotte L, Capecchi MR, Wellik DM: Hox patterning of the vertebrate rib cage. Development 2007, 134:2981-9.
[23] Ventura JJ, Kennedy NJ, Flavell RA, Davis RJ: JNK regulates autocrine expression of TGF-beta1. Mol Cell 2004, 15:269-78.
[24] Boswell CW, Ciruna B: Understanding idiopathic scoliosis: A new zebrafish school of thought. Trends Genet 2017, 33:183-96.
[25] Colombier P, Clouet J, Hamel O, Lescaudron L, Guicheux J: The lumbar intervertebral disc: from embryonic development to degeneration. Joint Bone Spine 2014, 81:125-9.

[26] Farrington-Rock C, Kirilova V, Dillard-Telm L, Borowsky AD, Chalk S, Rock MJ, Cohn DH, Krakow D: Disruption of the Flnb gene in mice phenocopies the human disease spondylocarpotarsal synostosis syndrome. Hum Mol Genet 2008, 17:631-41.
[27] Zieba J, Forlenza KN, Khatra JS, Sarukhanov A, Duran I, Rigueur D, Lyons KM, Cohn DH, Merrill AE, Krakow D: TGFbeta and BMP dependent cell fate changes due to loss of filamin B produces disc degeneration and progressive vertebral fusions. PLoS Genet 2016, 12:e1005936.
[28] Al Kaissi A, Ghachem MB, Nassib N, Ben Chehida F, Kozlowski K: Spondylocarpotarsal synostosis syndrome (with a posterior midline unsegmented bar). Skeletal Radiol 2005, 34:364-6.
[29] Campbell RM, Jr., Smith MD, Mayes TC, Mangos JA, Willey-Courand DB, Kose N, Pinero RF, Alder ME, Duong HL, Surber JL: The characteristics of thoracic insufficiency syndrome associated with fused ribs and congenital scoliosis. J Bone Joint Surg Am 2003, 85-A:399-408.
[30] Hensinger RN: Congenital scoliosis: etiology and associations. Spine (Phila Pa 1976) 2009, 34:1745-50.
[31] Tanaka T, Uhthoff HK: The pathogenesis of congenital vertebral malformations. A study based on observations made in 11 human embryos and fetuses. Acta Orthop Scand 1981, 52:413-25.

Figure Legends

Figure 1. Col2-Cre recombinase expression in E17.5 mouse embryos. The cells expressing Cre were identified by crossing *Col2-Cre* mice with ZsGreen reporter mice and performing immunohistochemistry with an antibody to detect ZsGreen. Positive cells (brown) were observed in developing long bones (elbow-**A, D, G, J**), vertebral column (**B, E, H, K**) that included nucleus pulposus (NP), inner annulus fibrosus (AF), cartilage end plate (CEP), and vertebral body (VB). Positive cells were also seen in the sternum and ribs (**C, F, I, L**). The elbow and vertebral column are shown in sagittal orientation, whereas the sternum is presented in the coronal plane. Black boxes in **A-C** show location of higher magnification images in **D-F,** respectively. Red boxes in **D-F** show location of higher magnification images in **G-I**, respectively, and purple boxes in **D-F** show location of higher magnification images in **J-L**, respectively. Scale bars = 20 µm; n=1.

Figure 2. Evaluation of the scoliotic phenotype in *JNK1/2* dKO and control mice. MicroCT analysis of whole skeleton in 4-week–old (**A, C**) and 10-week–old (**B, D**) *JNK1/2* dKO mice, compared to controls (CTRL-**B, D**) and Hets (**A, C**). High resolution microCT (18 µm) of caudal lumbar region (**C, D**). Red arrows point to fusions in transverse processes and yellow arrows to fusions of spinous processes; red asterisk marks vertebral fusions at the level of intervertebral disc (IVD). Alcian blue/Alizarin red staining of 10-week–old whole skeletons (**E**) and lumbosacral (**F**), thoracic (**G**), and cervical regions (**H**). Red arrows show vertebral fusions in the dKO whereas black arrows show similar locations in controls, yellow arrow shows cartilaginous fusion in the thoracic vertebrae. Dot plots of the mean ± SEM for comparisons of body weights between 10-week–old wild-type (WT) (n=4), CTRL (n=3), Het (n=5), and dKO (n=7) (**I**). Micro

CT analysis of lumbar scoliosis severity (Cobb angle) in 6-week–old CTRL/Het and dKO mice; dot plots of the mean ± SEM for comparisons between genotypes and sexes (male/CTRL- n=3; male/dKO-n=3; female/CTRL-n=4; female/dKO-n-=7) (**J**). Scale bars **A, B, E-H** = 5 mm, scale bars **C, D** = 1 mm; *$P \leq 0.05$, ***$P < 0.001$,****$P < 0.0001$.

Figure 3. JNK1 and 2 protein expression in the vertebral column. JNK1/2 immunoblotting in femoral head cartilage (FC), muscle, and intervertebral disc (IVD) tissues from 6-week–old WT, CTRL, and dKO mice. Total protein stain was used as a loading control (**A**). JNK1/2 immunohistochemistry in E17.5 vertebral column sections from WT (**B, E**), CTRL (**C, F**), and dKO (**D, G**) mice; insets in **B-D** show location of higher magnification images in **E-G**, respectively. NP= nucleus pulposus, AF= inner annulus fibrosus, and VB= vertebral body. Scale bars = 20µm; n=3.

Figure 4. Analysis of the rib cage, sternum, and spine in *JNK1/2* dKO and control mice. MicroCT analysis of rib cage and vertebral column of 11-day–old dKO and control (CTRL) mice. Red arrows point to fusions of the vertebrae at the level of the transverse processes and laminae and yellow arrows to fusions of spinous processes (**A**). Red asterisk points to fusions at the level of the intervertebral disc (IVD) (**B, C**). Alcian blue (**D, E**), and Alcian blue/Alizarin red staining (**F**) of E17.5 whole embryos. Red arrows point to fusions of the vertebrae dorsally (**E**) and black arrows point to mineralization centers at the level of spinous processes (**F**). Scale bars A-C = 1 mm, n=1; scale bars **D-F** = 5 mm; n=3.

Figure 5. Analysis of the intervertebral discs in the *JNK1/2* dKO and control mice. Safranin O/fast green stain showing 4 week–old (top and middle panels) and 10 week–old (bottom panels) thoracic (**A-H**) and lumbar spine (**I-X**) intervertebral discs (IVD), vertebral growth plate (GP), and cartilage endplate (CEP) from WT, CTRL, Het, and dKO in coronal orientation. Thoracic IVDs of 4-week–old dKO mice show strong proteoglycan (PG) stain surrounding a reduced area of nucleus pulposus (NP) (yellow arrow in **D**) and absence of AF lamellar structure. In some thoracic segments, a PG rich cartilaginous tissue connected the cranial and caudal vertebral growth plates (black arrow in **D**). In the lumbar IVDs of 4-week–old dKO mice, the NP was either very small (yellow arrows in **L, P**) or absent (not shown here) and both annulus fibrosus (AF) and NP were replaced by cartilaginous tissue. In 10 week–old dKO, most of AF and NP in distal thoracic (not shown here) and lumbar segments (**Q-X**) were replaced by areas of cartilage (white arrows in **T, X**) and bone (red arrows in **T, X**). Insets in **A-D** show location of higher magnification images in **E-H**, respectively; insets in **I-L** show location of higher magnification images in **M-P**; insets in **Q-T** show location of higher magnification images in **U-X**. Scale bars (**A-X**) = 20µm, n≥3.

Figure 6. Analysis of collagen fiber orientation in *JNK1/2* dKO and control mice. Picrosirius red stain (visualized under polarizing light) was used to visualize collagen in lumbar spine intervertebral discs (IVD) of 4 week–old WT, CTRL, Het, and dKO. Images show lack of organization of the collagen fibers in the annulus fibrosus (AF) laminae of dKO mice (**D, H**), whereas all the other genotypes showed concentrically aligned fibers in AF laminae (**A-C**, **E-G**). Yellow circles show location of higher magnification images in the bottom panels. Scale bars-20µm, n=3.

Figure 7. Evaluation of endochondral bone formation in *JNK1/2* dKO and control mice. Safranin O stain (**A, F**) shows replacement of intervertebral disc (IVD) tissues by bone (red arrow in **F**) and cartilage (black arrow in **F**) in 10-week–old dKO mice. Immunohistochemistry for type X collagen (**B, G**), as a marker of hypertrophic chondrocytes, for the cell cycle inhibitor p57 (also expressed by hypertrophic chondrocytes) (**C, H**), for Runx2 (**D, I**) (for hypertrophic chondrocytes and osteoblasts) and for PCNA, as a marker of cell proliferation (**E, J**). Higher magnification insets are included below their respective panels. NP- nucleus pulposus and AF- annulus fibrosus identified with the yellow arrows. Scale bars = 20µm, dKO, n=3; CTRL/Het, n=3.

Figure 8. Analysis of notochord development in *JNK1/2* dKO and control mice. Hematoxylin and eosin–stained sections of mouse embryos at E11.5 (**A-C**) and E13.5 (**D-F**) showing the presence of the notochord (red arrows) in all genotypes. The images represent sagittal sections through the whole embryo. IR= intervertebral regions; VR=vertebral regions. Insets show higher magnification of areas marked with the red arrow. Scale bars = 20µm, E11.5 dKO, n=3; CTRL/Het, n=4; E13.5 dKO, n=3; CTRL/Het, n=7.

Figure 9. Analysis of cell organization and collagen fiber orientation in *JNK1/2* dKO and control mice. Hematoxylin and eosin staining of E15.5 (**A-F**) and E17.5 (**G-L**) intervertebral disc (IVD) showing larger, unorganized cells in the inner annulus fibrosus (AF) of dKO mice (**C, F, I, L**) (red arrows in **F, L**) compared to control (CTRL) (**A, D, G, J**)) and Het littermates (**B, E,**

H, K)) (black arrows in **D, E, J, K**). Safranin O/fast green stain of E17.5 vertebral column (**M-O**) showing fusion of posterior spinal elements (black circles) in the dKO (**O**). The images represent sagittal sections through the vertebral column. SC= spinal cord. Boxes in **A-C** show location of higher magnification images in **D-F** and boxes in **G-I** show location of higher magnification images in **J-L**, respectively. Scale bars **A-C**, **G-I**, **M-O** = 20µm, scale bars **D-F**, **J-L** = 10µm; E15.5 dKO, n=5; CTRL/Het, n=6; E17.5 dKO, n=4; CTRL/Het, n=8.

Figure 10. Analysis of intervertebral disc (IVD) size in E17.5 embryo thoracic spine and 4-week–old tail in *JNK1/2* dKO and control mice. Dot plots of the mean ± SEM for comparisons of IVD components between E17.5 CTRL (n=6) and dKO (n=3). IVD measurements were taken at the level of two thoracic IVD: T10-T11 and T11-T12 in E17.5 dKO and CTRL mice and an AVG of the two segments was reported for vertebral GP length (**A**), ventral AF width (**B**), and NP width (**C**). Dot plots of the mean ± SEM for comparisons of proximal tail IVD measurements between 4-week–old WT (n=4), CTRL (n=6), and dKO (n=3), showing IVD width (**D**), NP height (**E**), and NP width (**F**). *$P \leq 0.05$, **$P < 0.01$.

Figure 11. Evaluation of sternum in 10-week–old *JNK1/2* dKO and control mice. Alcian blue/Alizarin red staining showing the presence of a cartilaginous tissue (blue stain, yellow circles) between sternebrae in the *JNK1/2* dKO mice (**A, B**). Boxes in **A, B** show location of higher magnification images in the adjacent panels. Safranin O/fast green staining showing a tissue rich in proteoglycans between sternebrae (**C, D**) and the expansion of this cartilaginous

tissue in the dKO (**B**). GP = growth plate. Scale bars **A, B** = 5mm (higher magnification panels, scale bars =2.5 mm), scale bars **C, D** = 20µm; dKO, n=5; CTRL/Het, n=4.

Figure 12. Analysis of embryonic tibia and 10-week–old knee joints in *JNK1/2* dKO and control mice. Safranin O/fast green staining showing E17.5 tibia growth plate (GP) and mineralized regions (Min) (**A-C**). Dot plots of the mean ± SEM for comparisons of tibia GP and Min regions between E17.5 CTRL (n=4), Het (n=4), and dKO (n=4) (**D**). Safranin O/fast green staining showing 10-week–old knee joint sections (**E-G**). Dot plots of the mean ± SEM for comparisons of knee joint width (**H**), articular cartilage (AC) thickness (**I**), and tibial plateau [AC+GP+ subchondral bone (SB)] thickness (**J**) between 10-week–old wild-type (WT) (n=4), CTRL (n=3), and dKO (n=4) (**D**). Scale bars = 20µm; $*P \leq 0.05$, $**P < 0.01$.

Figure 13. P-c-Jun immunohistochemical staining of E 17.5 *JNK1/2* dKO and control intervertebral discs (IVDs) and evaluation of apoptosis in vertebral column sections from E11.5 and E13.5 *JNK1/2* dKO and control mice. Immunohistochemistry for phospho-c-Jun (**A, B**) in lumbar IVDs from E 17.5 *JNK1/2* dKO and CTRL embryos. There is positive stain in the spinal cord (SC) and other tissues adjacent to the vertebral column in both genotypes. The images represent sagittal sections through the vertebral column. The positive immunostain is brown and the slides were counterstained with methyl green. Insets in **A** and **B** show location of higher magnification images in the adjacent panels. Scale bars = 20µm; dKO, n=3; CTRL/Het, n=3. TUNEL positive cells (brown, red arrows) can be noticed around notochord regions (in the perinotochordal sclerotome) and at the level of high cell density (condensations) in the vertebral

column at E11.5 in all genotypes: CTRL, Het, and dKO (**C-E**). At E13.5, the positive cells were localized mostly within the notochord (**F-H**). Boxes show location of higher magnification images in the adjacent panels. Scale bars = 20μm, dKO, n=3; CTRL, n=3. Dot plots of the mean ± SEM for comparisons of number of TUNEL positive cells per condensation (**I**), in the perinotochordal sclerotome (**J**) and within the notochord (**K**) between E11.5 control (CTRL and Het were pooled for analysis) and dKO; dKO, n=3; CTRL/Het, n=3.

Table 1. Number of animals analyzed and scoliosis phenotype distribution.

Genotype	Scoliosis phenotype observed	Male	Female
JNK1$^{fl/fl}$*Col2-Cre*/*JNK2*$^{-/-}$ (dKO)	37 of 37	18 of 18	19 of 19
JNK1$^{fl/fl}$/*JNK2*$^{-/-}$ (CTRL)	0 of 60	0 of 29	0 of 31
JNK1$^{fl/WT}$*Col2-Cre*/*JNK2*$^{-/-}$ (Het)	0 of 49	0 of 23	0 of 26
JNK1$^{fl/WT}$/*JNK2*$^{-/-}$ (CTRL)	0 of 76	0 of 43	0 of 33
Total number of mice analyzed	222	113	109

Elbow joint

Vertebral column

Sternum and ribs

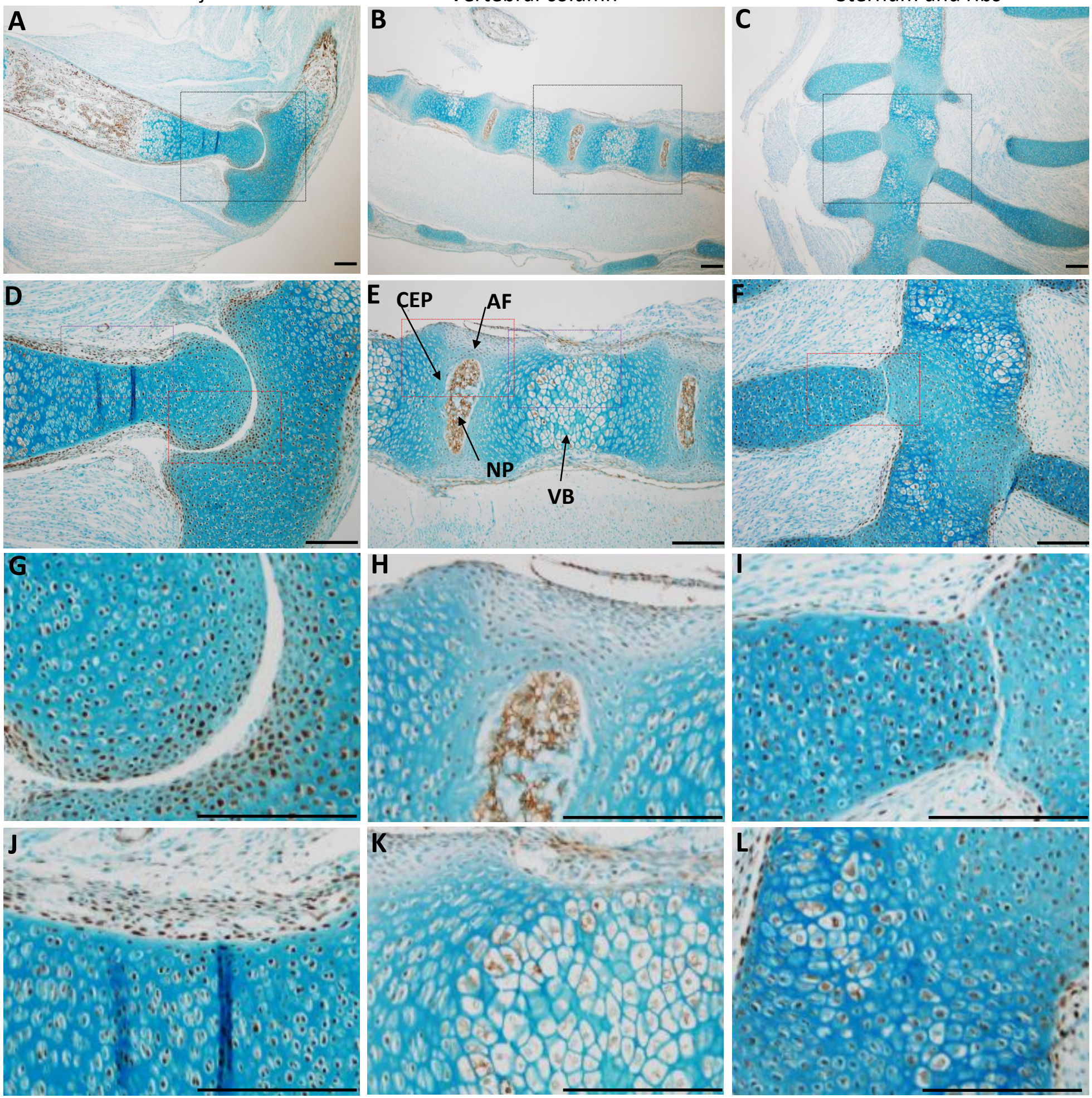

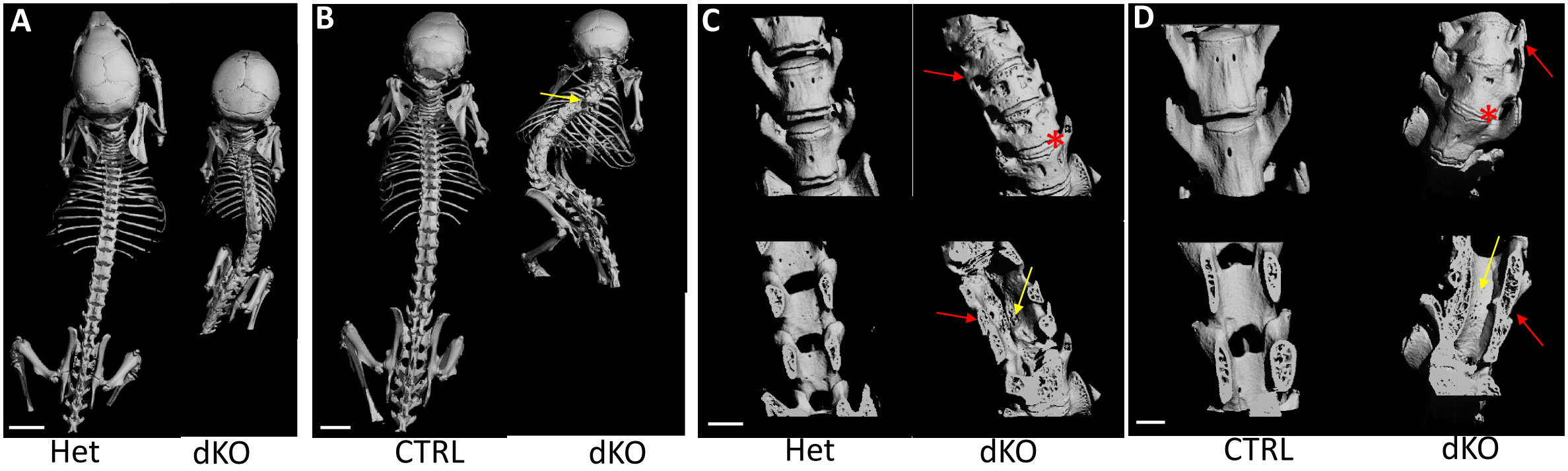
A
B
C
D
Het
dKO
CTRL
dKO
Het
dKO
CTRL
dKO

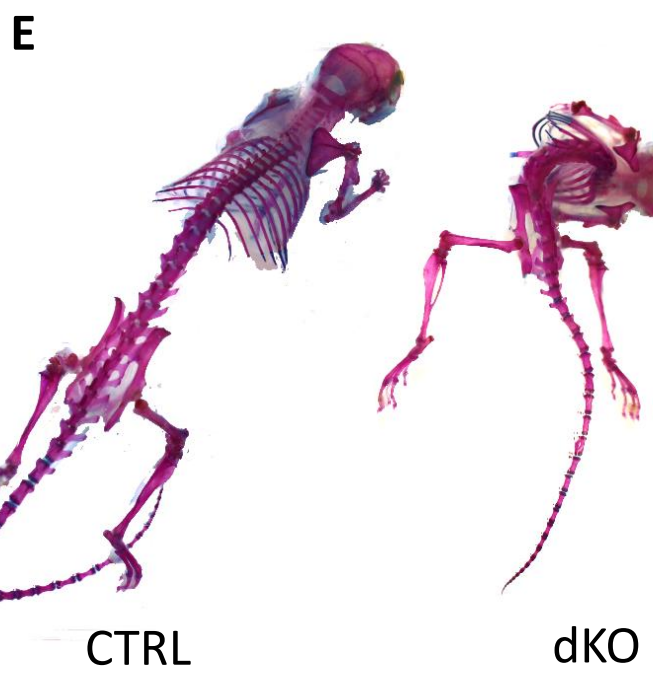
E
CTRL
dKO

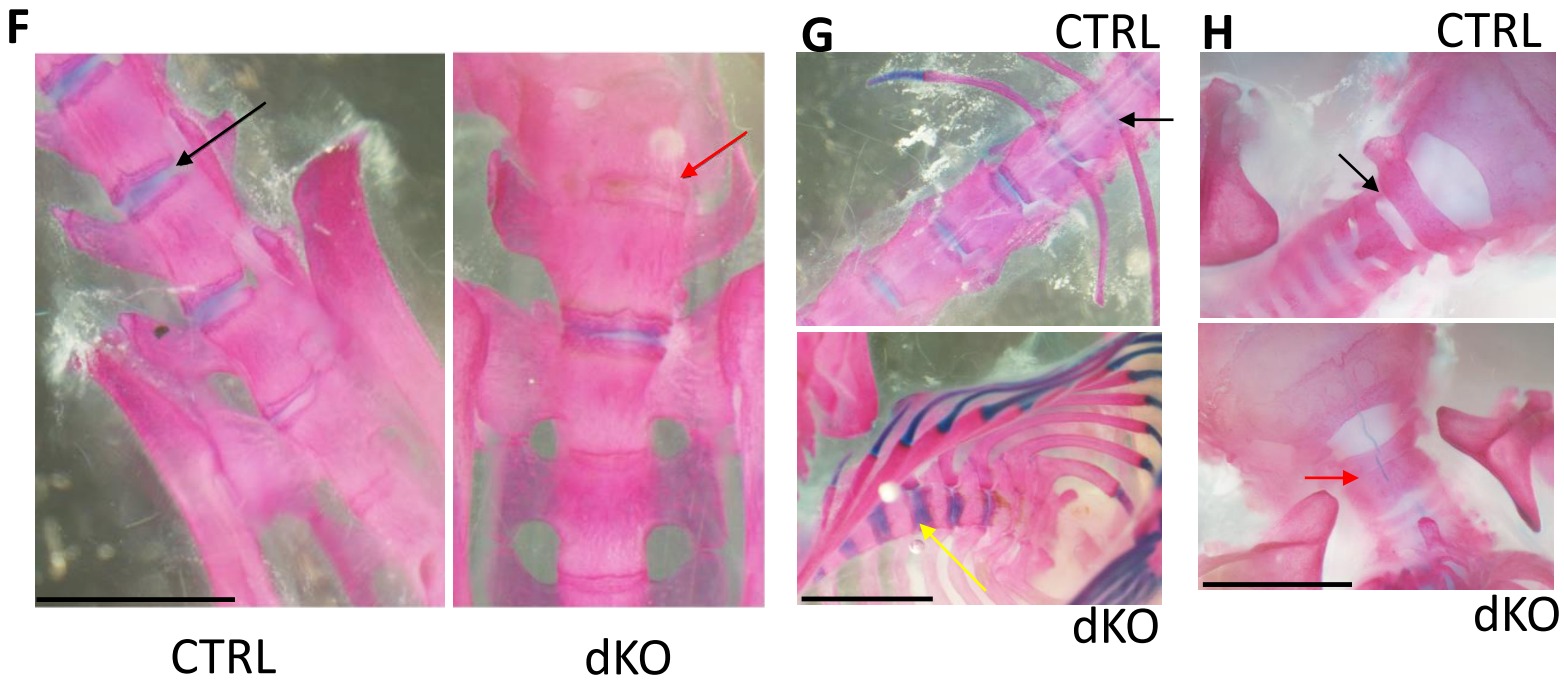
F
G
CTRL
H
CTRL
CTRL
dKO
dKO
dKO

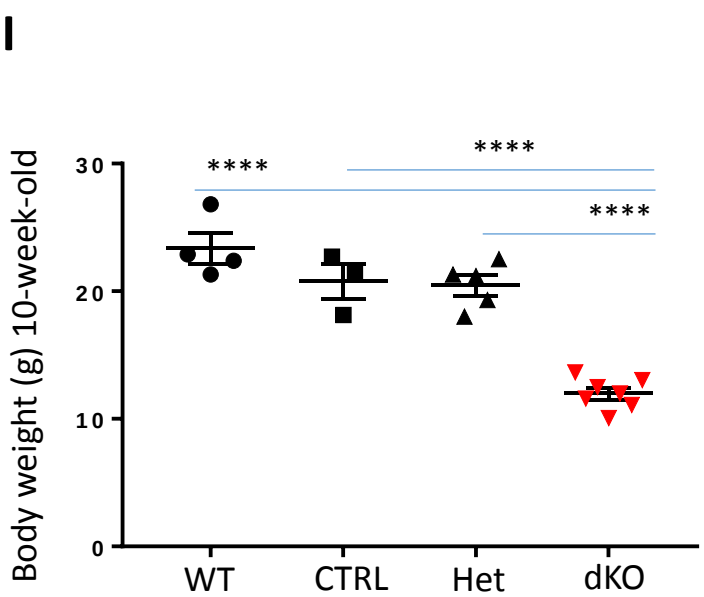
I
Body weight (g) 10-week-old
30
20
10
0
****
****
****
WT
CTRL
Het
dKO

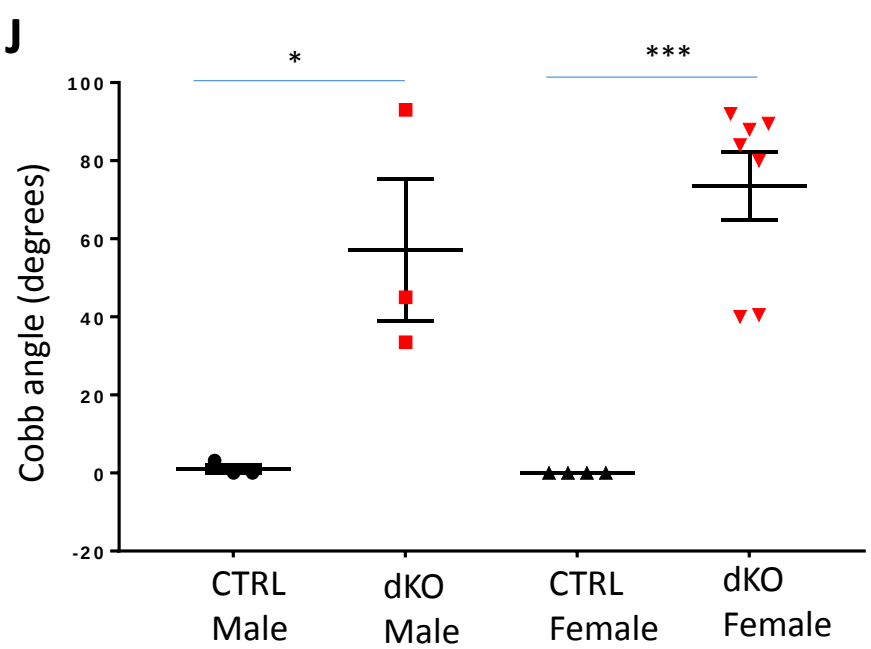
J
Cobb angle (degrees)
100
80
60
40
20
0
-20
*
***
CTRL Male
dKO Male
CTRL Female
dKO Female

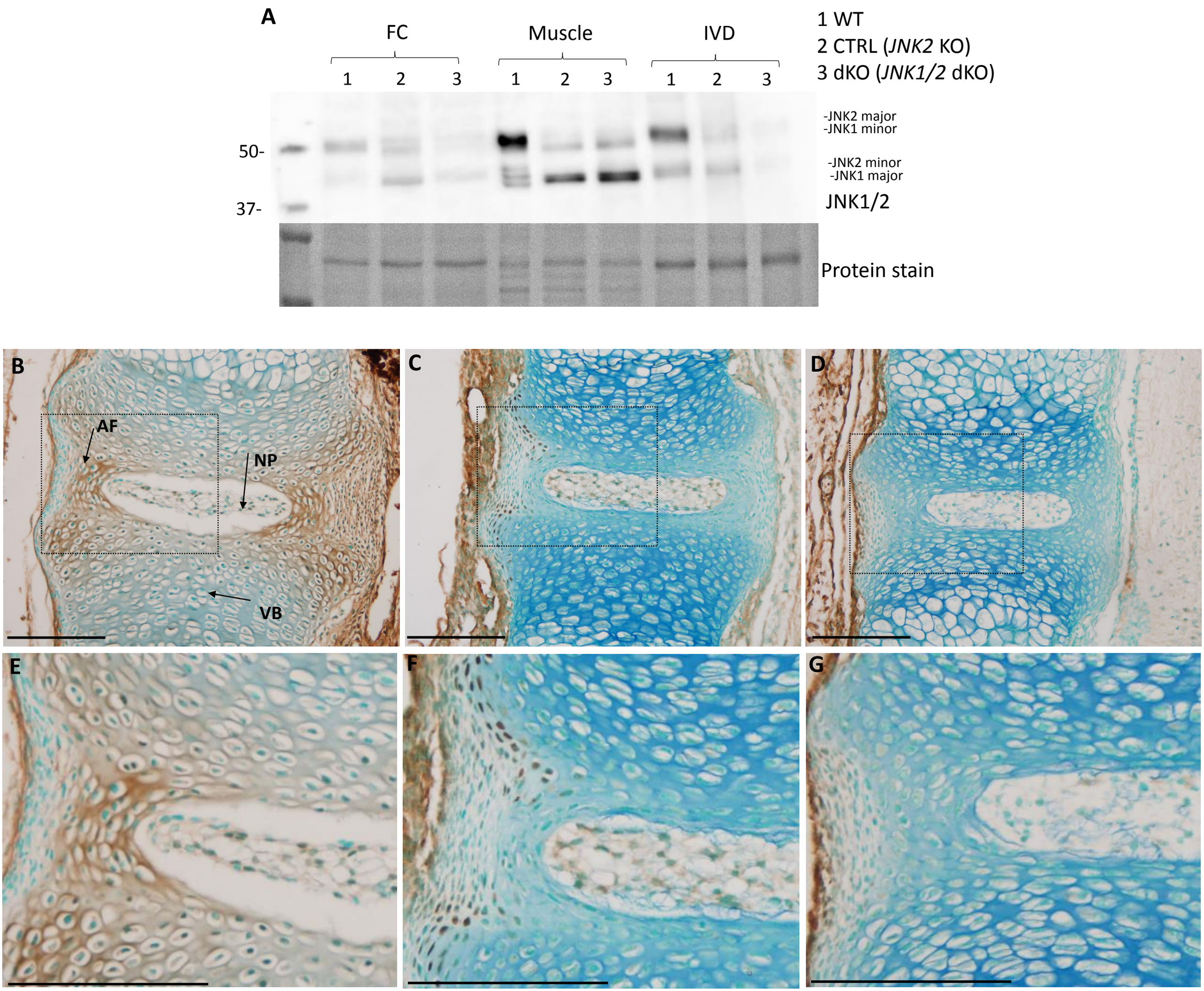
A
FC
Muscle
IVD
1 2 3 1 2 3 1 2 3
1 WT
2 CTRL (JNK2 KO)
3 dKO (JNK1/2 dKO)
50-
37-
-JNK2 major
-JNK1 minor
-JNK2 minor
-JNK1 major
JNK1/2
Protein stain
B
AF
NP
VB
C
D
E
F
G

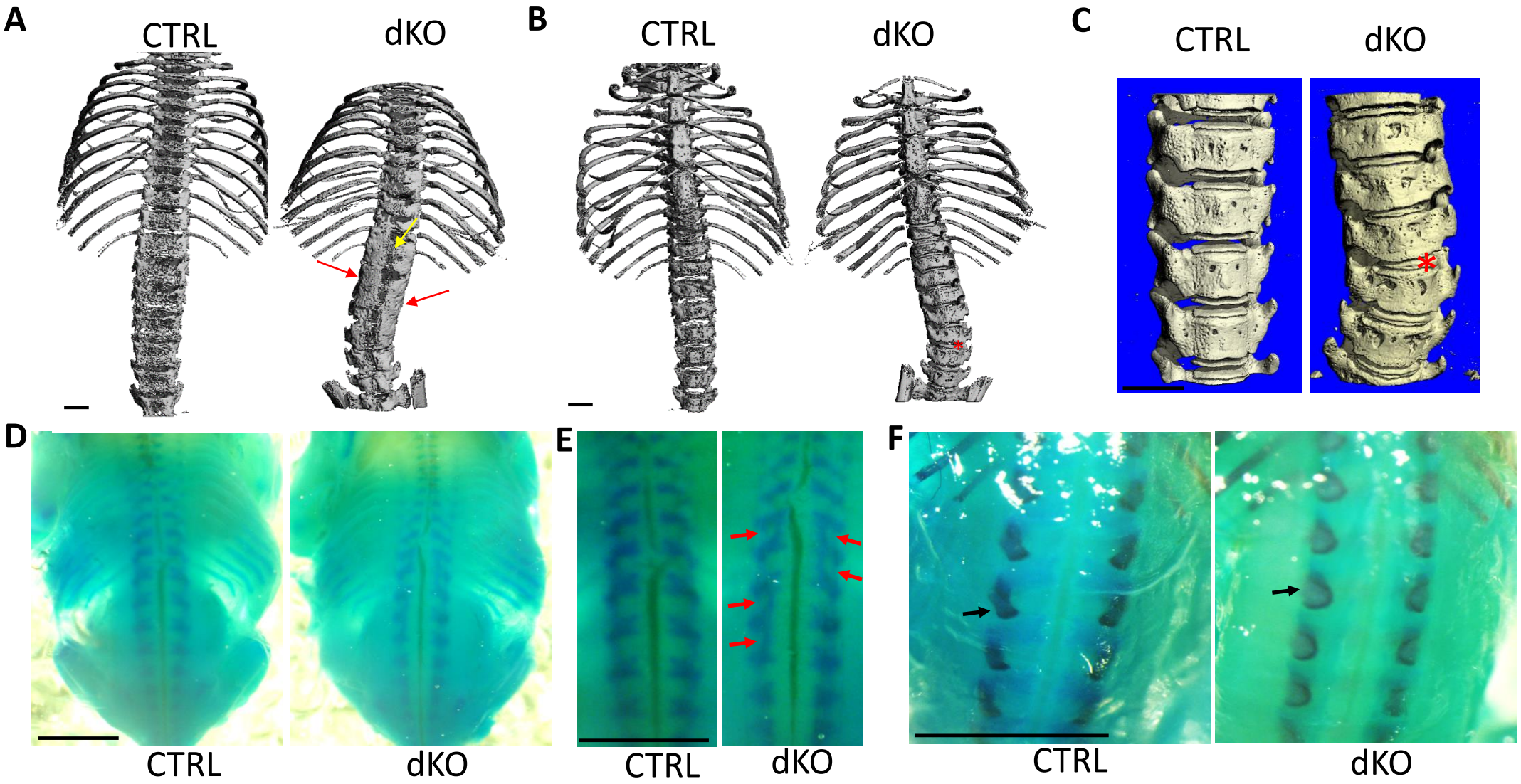
A
CTRL
dKO
B
CTRL
dKO
C
CTRL
dKO
D
CTRL
dKO
E
CTRL
dKO
F
CTRL
dKO

WT
CTRL
Het
dKO
Thoracic 4wo
A
B
C
D
E
F
G
H
Thoracic 4wo
WT
CTRL
Het
dKO
Lumbar 4wo
I
J
K
L
CEP
AF
NP
GP
M
N
O
P
Lumbar 4wo
WT
CTRL
Het
dKO
Lumbar 10wo
Q
R
S
T
U
V
W
X
Lumbar 10wo

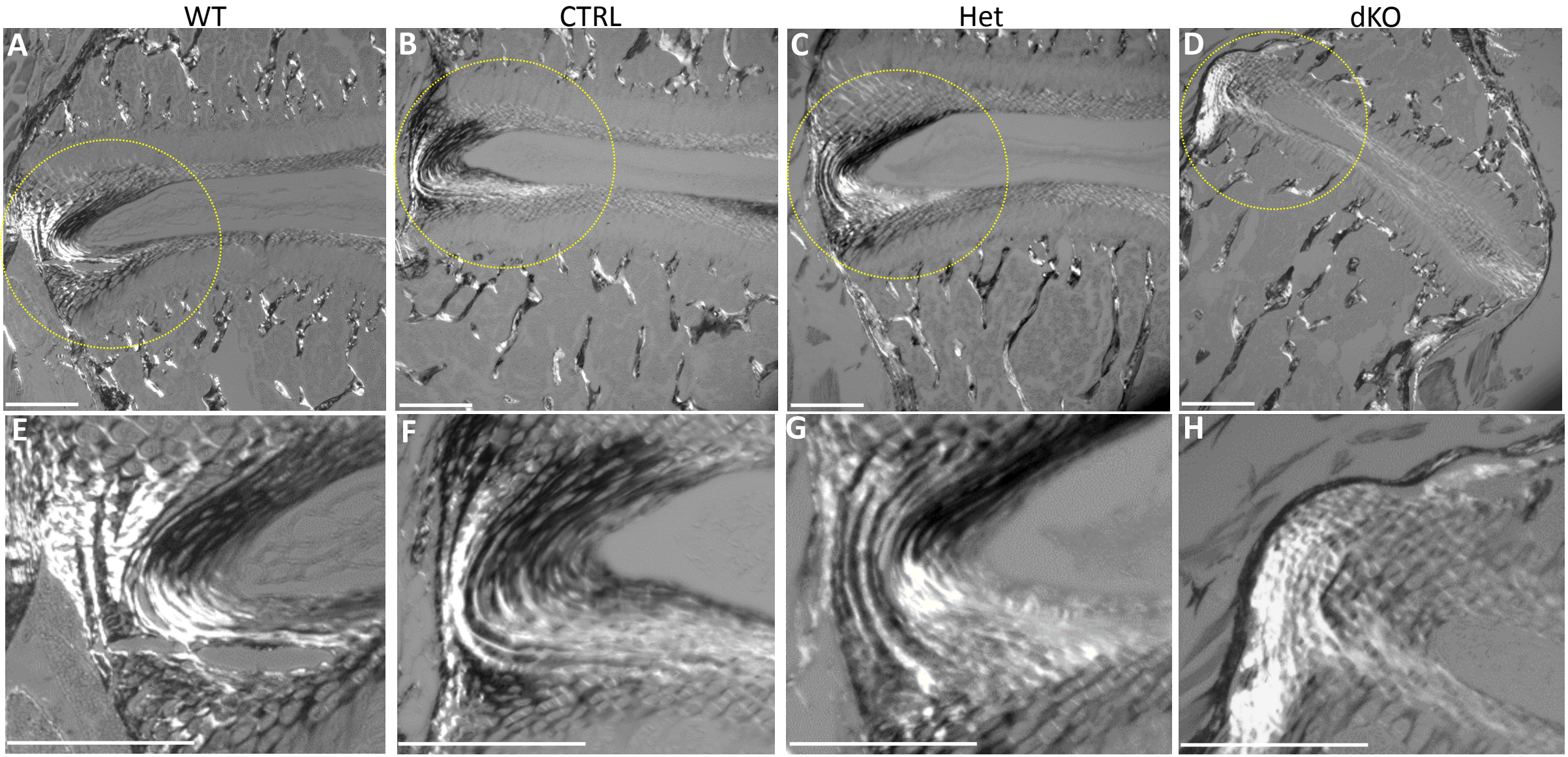
WT
CTRL
Het
dKO
A
B
C
D
E
F
G
H

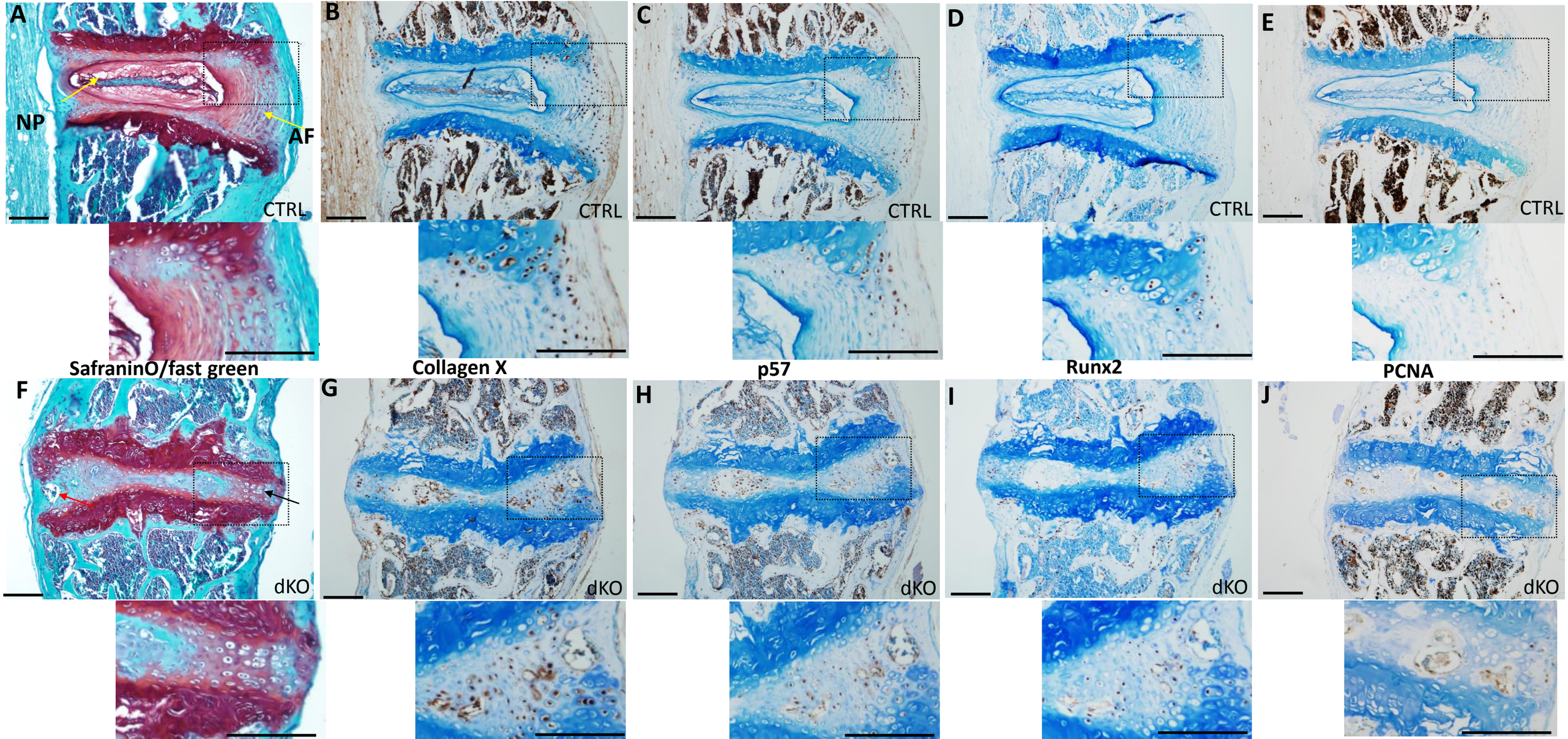
A
NP
AF
CTRL
B
CTRL
C
CTRL
D
CTRL
E
CTRL
SafraninO/fast green
Collagen X
p57
Runx2
PCNA
F
dKO
G
dKO
H
dKO
I
dKO
J
dKO

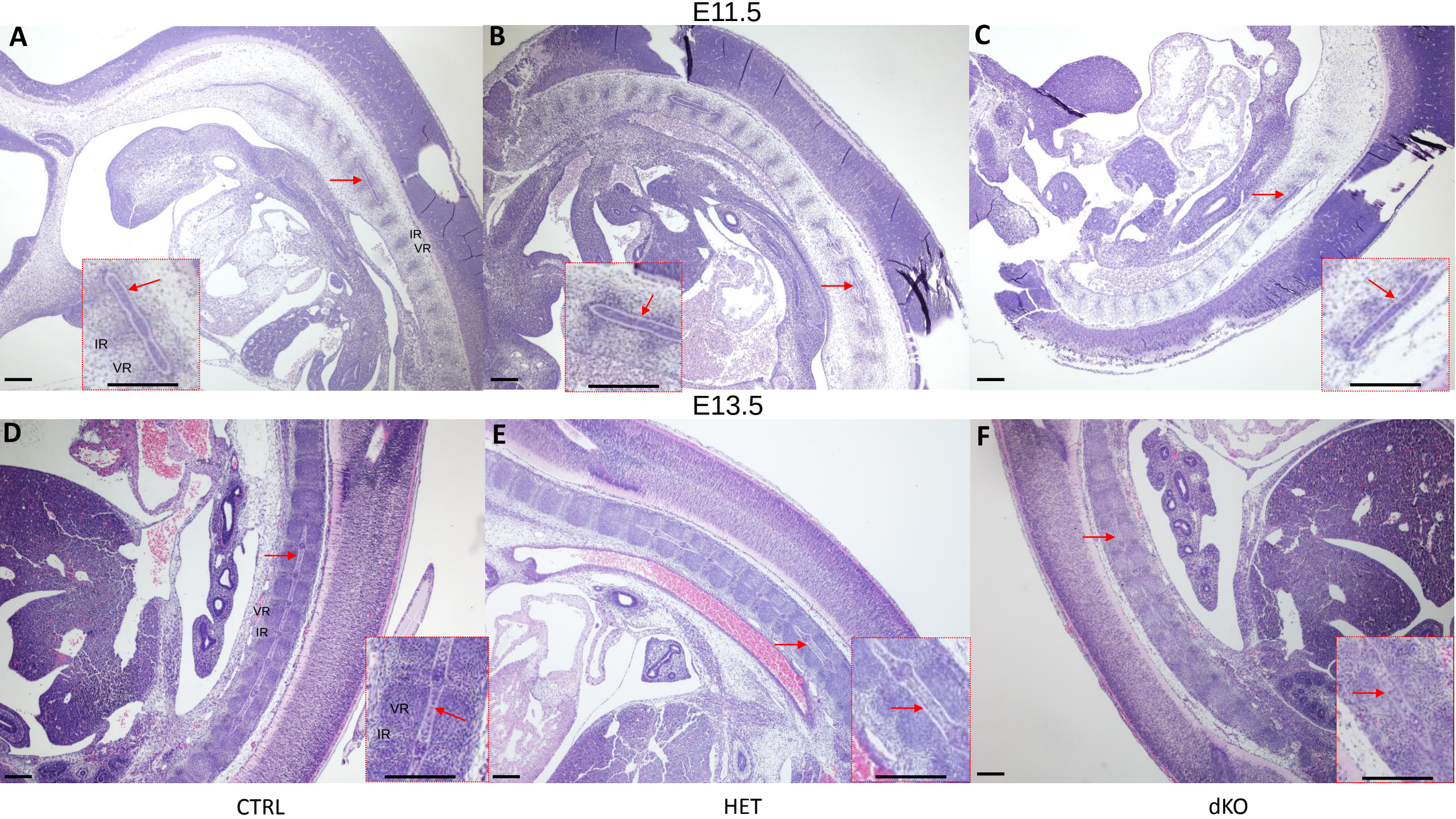
E11.5
A
B
C
IR
VR
IR
VR
E13.5
D
E
F
VR
IR
VR
IR
CTRL
HET
dKO

CTRL

Het

dKO

A

SC

B

SC

C

SC

D

E

F

G

SC

H

SC

I

SC

J

K

L

M

SC

N

SC

O

SC

Vertebral bodies- E17.5

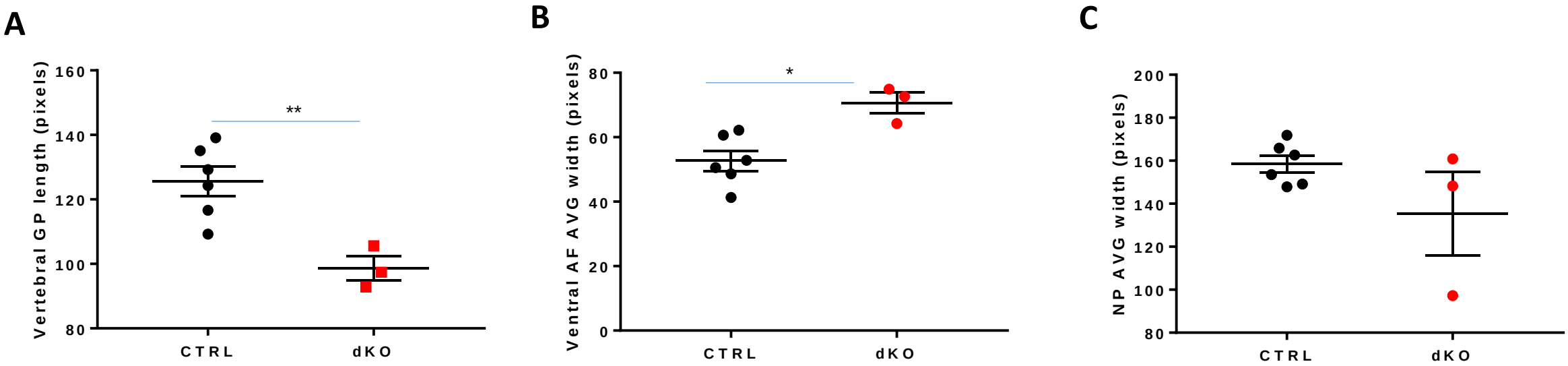

Tail IVD- 4 weeks old

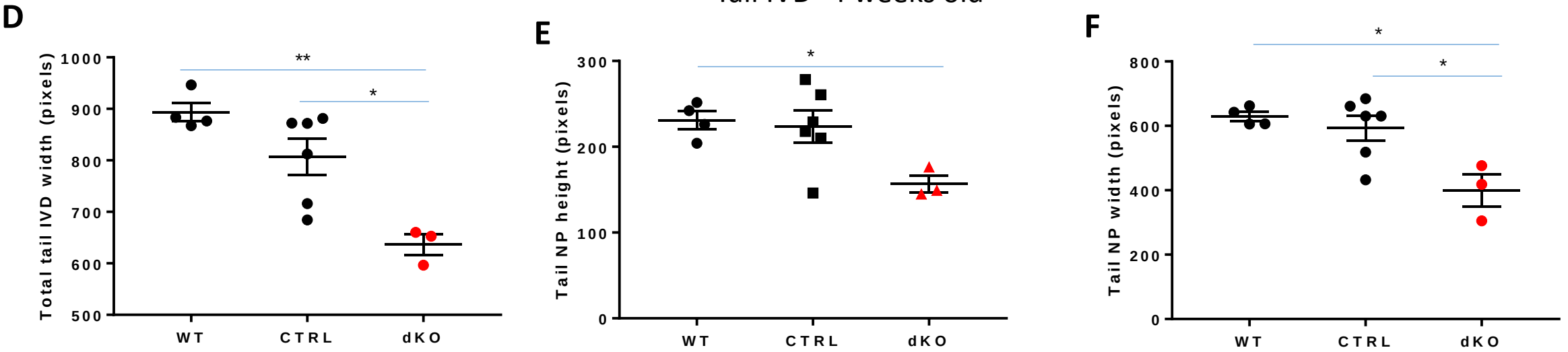

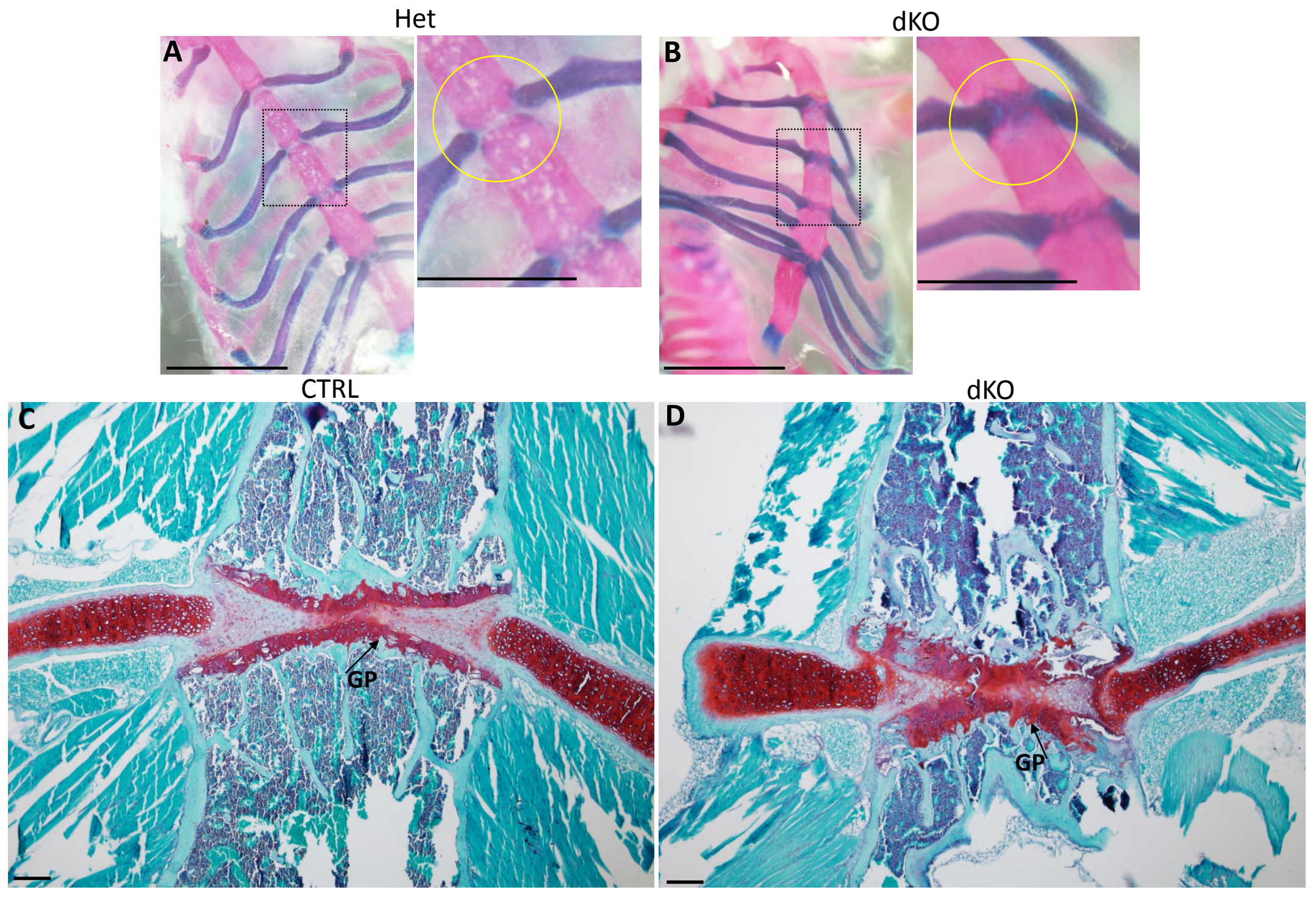
Het
dKO
A
B
CTRL
dKO
C
D
GP
GP

CTRL

Het

dKO

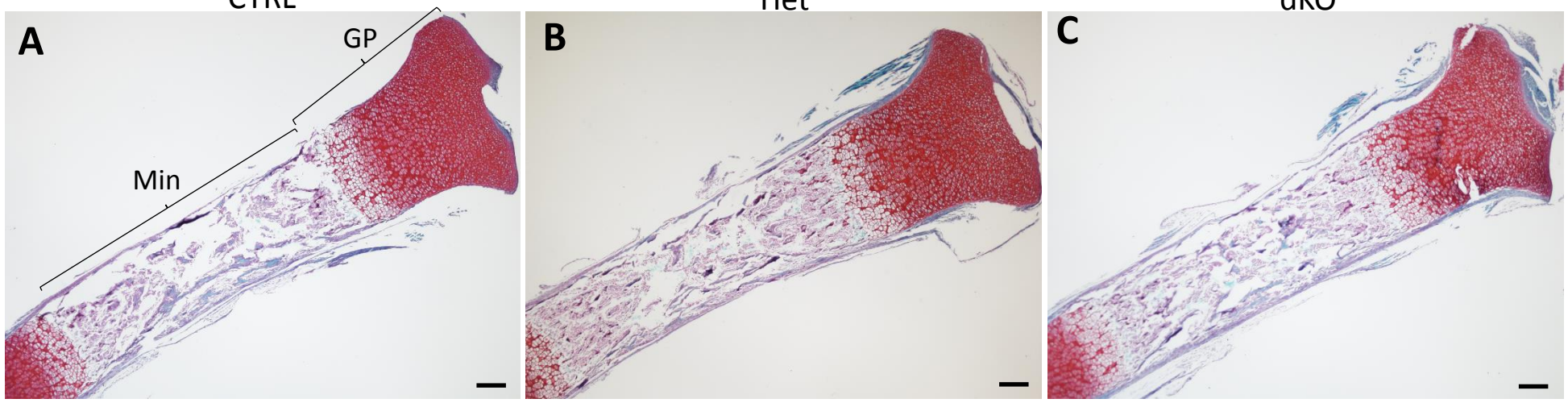

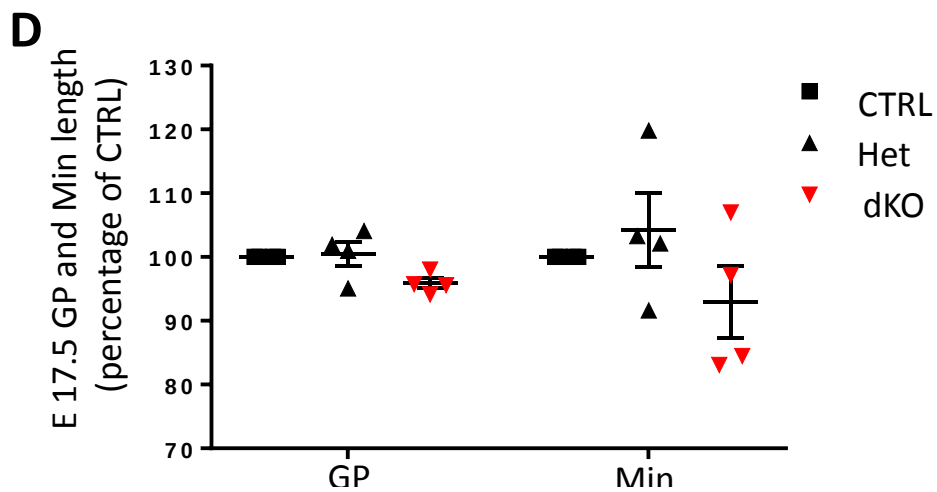

CTRL

Het

dKO

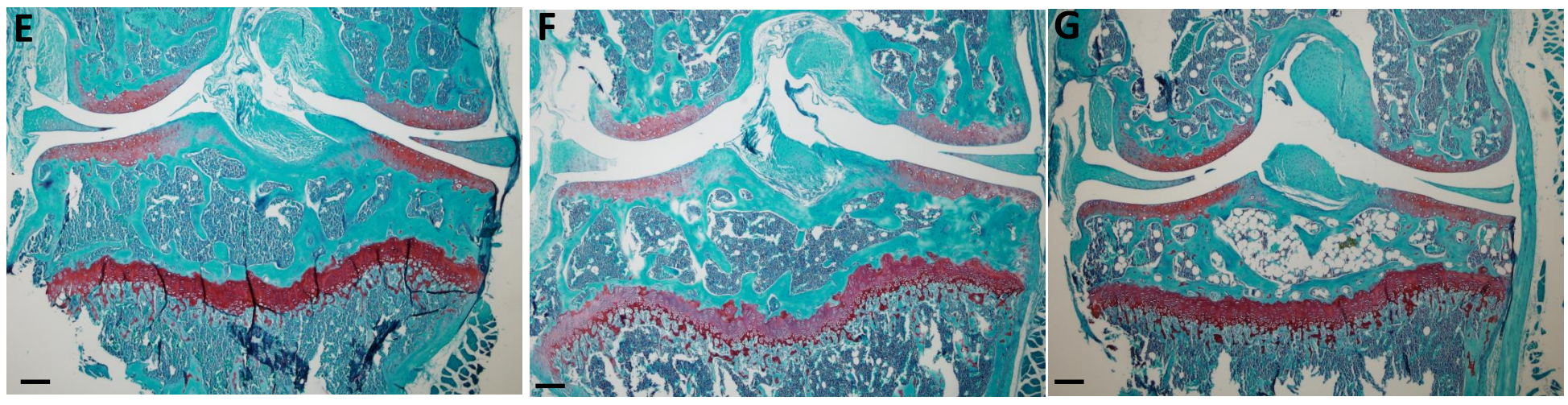

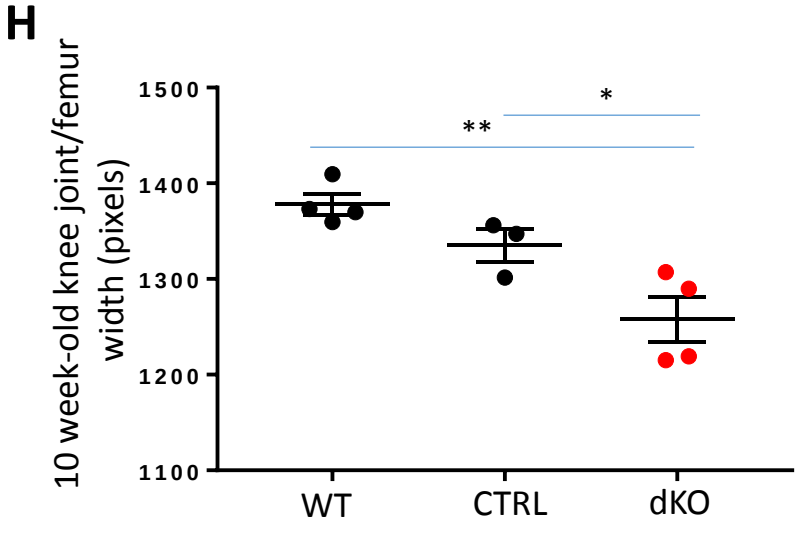

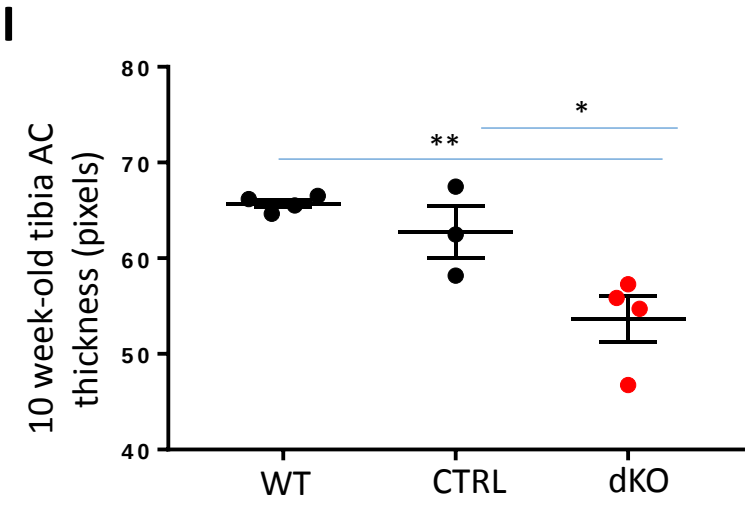

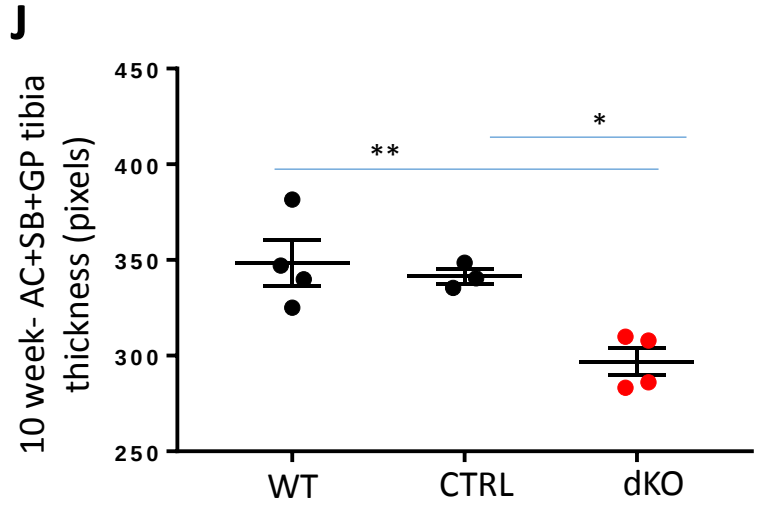

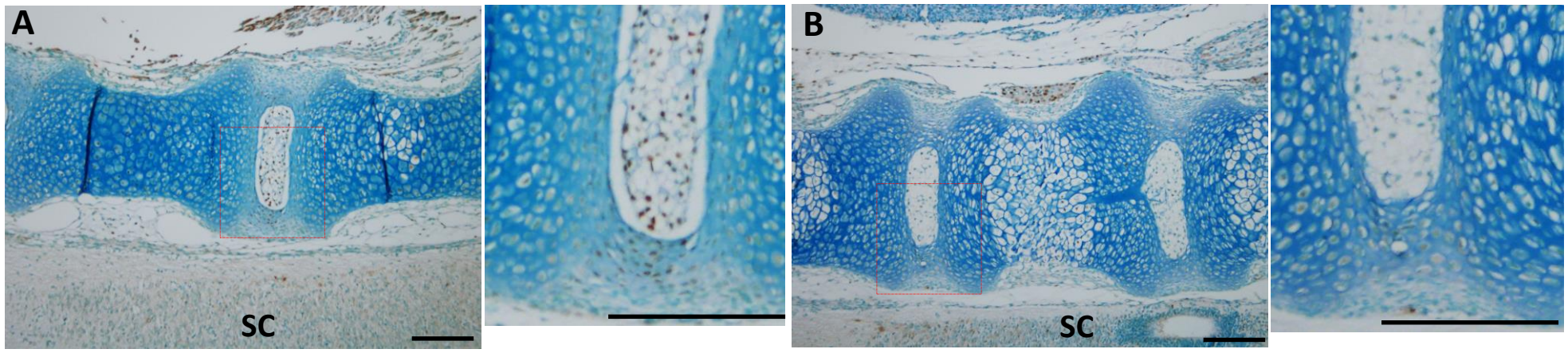

P-c-Jun
E17.5

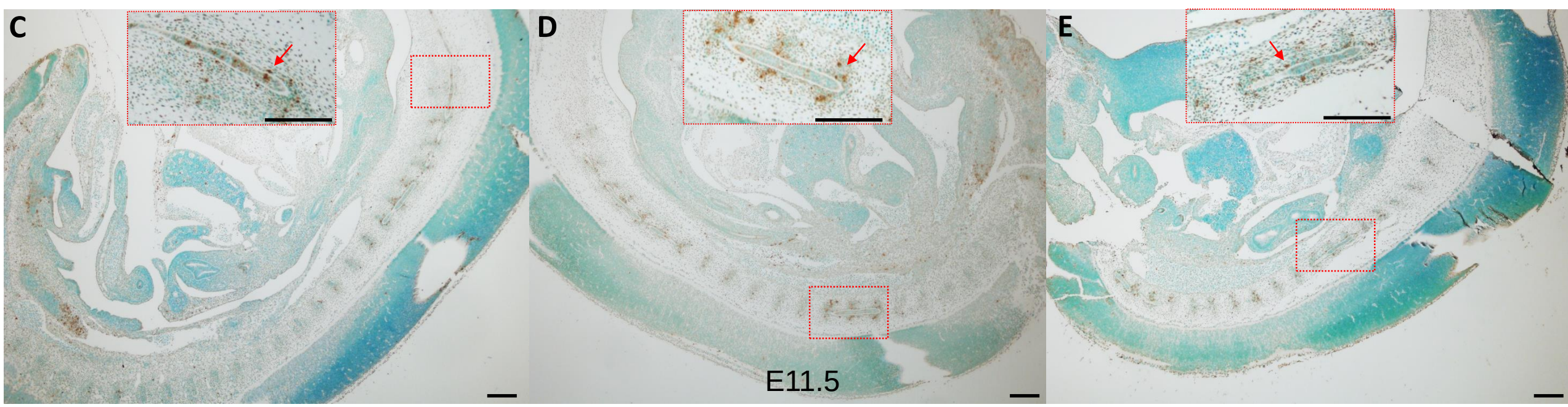

CTRL HET dKO